ARTICLE

doi:10.1038/nature13777

Reversion of advanced Ebola virus disease in nonhuman primates with ZMapp

Xiangguo Qiu[1], Gary Wong[1,2], Jonathan Audet[1,2], Alexander Bello[1,2], Lisa Fernando[1], Judie B. Alimonti[1], Hugues Fausther-Bovendo[1,2], Haiyan Wei[1,3], Jenna Aviles[1], Ernie Hiatt[4], Ashley Johnson[4], Josh Morton[4], Kelsi Swope[4], Ognian Bohorov[5], Natasha Bohorova[5], Charles Goodman[5], Do Kim[5], Michael H. Pauly[5], Jesus Velasco[5], James Pettitt[6]†, Gene G. Olinger[6]†, Kevin Whaley[5], Bianli Xu[3], James E. Strong[1,2,7], Larry Zeitlin[5] & Gary P. Kobinger[1,2,8,9]

Without an approved vaccine or treatment, Ebola outbreak management has been limited to palliative care and barrier methods to prevent transmission. These approaches, however, have yet to end the 2014 outbreak of Ebola after its prolonged presence in West Africa. Here we show that a combination of monoclonal antibodies (ZMapp), optimized from two previous antibody cocktails, is able to rescue 100% of rhesus macaques when treatment is initiated up to 5 days post-challenge. High fever, viraemia and abnormalities in blood count and blood chemistry were evident in many animals before ZMapp intervention. Advanced disease, as indicated by elevated liver enzymes, mucosal haemorrhages and generalized petechia could be reversed, leading to full recovery. ELISA and neutralizing antibody assays indicate that ZMapp is cross-reactive with the Guinean variant of Ebola. ZMapp exceeds the efficacy of any other therapeutics described so far, and results warrant further development of this cocktail for clinical use.

Ebola virus (EBOV) infections cause severe illness in humans, and after an incubation period of 3 to 21 days, patients initially present with general flu-like symptoms before a rapid progression to advanced disease characterized by haemorrhage, multiple organ failure and a shock-like syndrome[1]. In the spring of 2014, a new EBOV variant emerged in the West African country of Guinea[2], an area in which EBOV had not been previously reported. Despite a sustained international response from local and international authorities including the Ministry of Health (MOH), World Health Organization (WHO) and Médecins Sans Frontières (MSF) since March 2014, the outbreak has yet to be brought to an end after five months. As of 15 August 2014, there are 2,127 total cases and 1,145 deaths spanning Guinea, Sierra Leone, Liberia and Nigeria[3]. So far, this outbreak has set the record for the largest number of cases and fatalities, in addition to geographical spread[4]. Controlling an EBOV outbreak of this magnitude has proven to be a challenge and the outbreak is predicted to last for at least several more months[5]. In the absence of licensed vaccines and therapeutics against EBOV, there is little that can be done for infected patients outside of supportive care, which includes fluid replenishment, administration of antivirals, and management of secondary symptoms[6,7]. With overburdened personnel, and strained local and international resources, experimental treatment options cannot be considered for compassionate use in an orderly fashion at the moment. However, moving promising strategies forward through the regulatory process of clinical development has never been more urgent.

Over the past decade, several experimental strategies have shown promise in treating EBOV-challenged nonhuman primates (NHPs) after infection. These include recombinant human activated protein C (rhAPC)[8], recombinant nematode anticoagulant protein c2 (rNAPc2)[9], small interfering RNA (siRNA)[10], positively-charged phosphorodiamidate morpholino oligomers (PMO*plus*)[11], the vesicular stomatitis virus vaccine (VSVΔG-EBOVGP)[12], as well as the monoclonal antibody (mAb) cocktails MB-003 (consisting of human or human–mouse chimaeric mAbs c13C6, h13F6 and c6D8)[13] and ZMAb (consisting of murine mAbs m1H3, m2G4 and m4G7)[14]. Of these, only the antibody-based candidates have demonstrated substantial benefits in NHPs when administered greater than 24 h past EBOV exposure. Follow-up studies have shown that MB-003 is partially efficacious when administered therapeutically after the detection of two disease "triggers"[15], and ZMAb combined with an adenovirus-based adjuvant provides full protection in rhesus macaques when given up to 72 h after infection[16].

The current objective is to develop a therapeutic superior to both MB-003 and ZMAb, which could be used for outbreak patients, primary health-care providers, as well as high-containment laboratory workers in the future. This study aims to first identify an optimized antibody combination derived from MB-003 and ZMAb components, before determining the therapeutic limit of this mAb cocktail in a subsequent experiment. To extend the antibody half-life in humans and to facilitate clinical acceptance, the individual murine antibodies in ZMAb were first chimaerized with human constant regions (cZMAb; components: c1H3, c2G4 and c4G7). The cZMAb components were then produced in *Nicotiana benthamiana*[17], using the large-scale, Current Good Manufacturing Practice-compatible Rapid Antibody Manufacturing Platform (RAMP) and magnICON vectors that currently also manufactures the individual components of cocktail MB-003, before efficacy testing in animals.

Selecting for the best mAb combinations

Our efforts to down-select for an improved mAb cocktail comprising components of MB-003 and ZMAb began with the testing of individual MB-003 antibodies in guinea pigs and NHPs. In guinea pig studies, animals were given one dose of mAb c13C6, h13F6 or c6D8 individually (totalling 5 mg per animal) at 1 day post-infection (dpi) with 1,000 × LD_{50} (median lethal dose) of guinea pig-adapted EBOV, Mayinga variant

[1]National Laboratory for Zoonotic Diseases and Special Pathogens, Public Health Agency of Canada, Winnipeg, Manitoba R3E 3R2, Canada. [2]Department of Medical Microbiology, University of Manitoba, Winnipeg, Manitoba R3E 0J9, Canada. [3]Institute of Infectious Disease, Henan Centre for Disease Control and Prevention, Zhengzhou, 450012 Henan, China. [4]Kentucky BioProcessing, Owensboro, Kentucky 42301, USA. [5]Mapp Biopharmaceutical Inc., San Diego, California 92121, USA. [6]United States Army Medical Research Institute of Infectious Diseases (USAMRIID), Frederick, Maryland 21702, USA. [7]Department of Pediatrics and Child Health, University of Manitoba, Winnipeg, Manitoba R3A 1S1, Canada. [8]Department of Immunology, University of Manitoba, Winnipeg, Manitoba R3E 0T5, Canada. [9]Department of Pathology and Laboratory Medicine, University of Pennsylvania School of Medicine, Philadelphia, Pennsylvania 19104, USA. †Present address: Integrated Research Facility, National Institute of Allergy and Infectious Diseases, National Institutes of Health, Frederick, Maryland 21702, USA.

Table 1 | Efficacy of individual and combined monoclonal antibody treatments in guinea pigs and nonhuman primates

Treatment groups, time of treatment	Dose (mg)	Mean time to death (days ± s.d.)	No. survivors/total	Survival (%)	Weight loss (%)	*P* value, compared with	
						cZMAb	MB-003
Guinea pigs						–	–
PBS, 3 dpi	N/A	7.3 ± 0.5	0/4	0	9%	–	–
cZMAb, 3 dpi	5	11.6 ± 1.8	1/6	17	7%	–	–
MB-003, 3 dpi	5	8.2 ± 1.5	0/6	0	40%	–	–
ZMapp1, 3 dpi	5	9.0 ± 0.0	4/6	67	<5%	0.190	0.0147
ZMapp2, 3 dpi	5	8.3 ± 0.6	3/6	50	8%	0.634	0.0692
ZMapp3, 3 dpi	5	8.6 ± 1.1	1/6	17	9%	0.224	0.411
c13C6, 1 dpi	5	8.4 ± 1.7	1/6	17	9%	–	–
h13F6, 1 dpi	5	10.2 ± 1.8	1/6	17	21%	–	–
c6D8, 1 dpi	5	10.5 ± 2.2	0/6	0	38%	–	–
Nonhuman primates							
PBS, 1 dpi	N/A	8.4 ± 1.9	0/1	0			
MB-003, 1 dpi	50	14.0 ± 2.8	1/3	33			
c13C6, 1 dpi	50	9.0 ± 1.4	1/3	33			
h13F6, 1 dpi	50	9.0 ± 2.0	0/3	0			
c6D8, 1 dpi	50	9.7 ± 0.6	0/3	0			

(EBOV-M-GPA). Survival and weight loss were monitored over 28 days. Treatment with c13C6 or h13F6 yielded 17% survival (1 of 6 animals) with a mean time to death of 8.4 ± 1.7 and 10.2 ± 1.8 days, respectively. The average weight loss for c13C6 or h13F6-treated animals was 9% and 21% (Table 1). In nonhuman primates, animals were given three doses of mAb c13C6, h13F6 or c6D8, beginning at 24 h after challenge with the Kikwit variant of EBOV (EBOV-K)[18], and survival was monitored over 28 days. Only c13C6 treatment yielded any survivors, with 1 of 3 animals protected from EBOV challenge (Table 1), confirming in two separate animal models that c13C6 is the component that provides the highest level of protection in the MB-003 cocktail.

We then tested mAb c13C6 in combination with two of three mAbs from ZMAb in guinea pigs. The individual antibodies composing ZMAb were originally chosen for protection studies based on their *in vivo* protection of guinea pigs against EBOV-M-GPA[19], and all three possible combinations were tested: ZMapp1 (c13C6+c2G4+c4G7), ZMapp2 (c13C6+c1H3+c2G4) and ZMapp3 (c13C6+c1H3+c4G7), and compared to the originator cocktails ZMAb and MB-003. Three days after

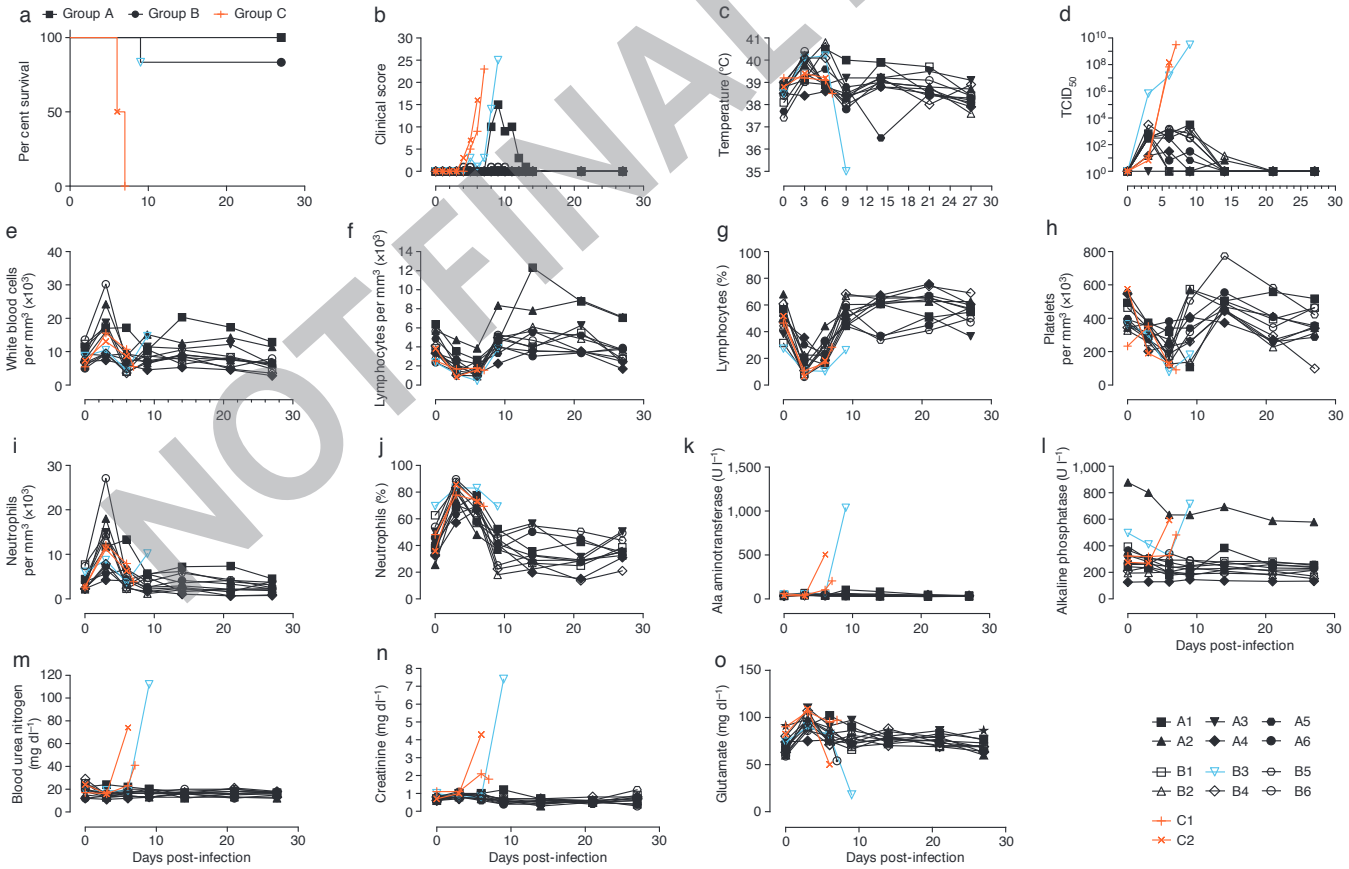

Figure 1 | Post-exposure protection of EBOV-infected nonhuman primates with ZMapp1 and ZMapp2. Rhesus macaques were challenged with EBOV-K, and 50 mg kg^{-1} of ZMapp1 (Group A) or ZMapp2 (Group B) were administered on days 3, 6, and 9 ($n = 6$ per treatment group, $n = 2$ for controls). Non-specific IgG mAb or PBS was administered as a control (Group C). a, Kaplan–Meier survival curves (log-rank tests: Group A vs Group C $P = 0.0039$; Group B vs Group C $P = 0.0039$). b, Clinical score. c, Rectal temperature. d, EBOV viraemia by $TCID_{50}$. Blood parameters: e, white blood cell count; f, lymphocyte count; g, lymphocyte percentage; h, platelet count; i, neutrophil count; j, neutrophil percentage; k, alanine aminotransferase; l, alkaline phosphatase; m, blood urea nitrogen; n, creatinine; o, glucose.

challenge with 1,000 × LD_{50} of EBOV-M-GPA, the animals received a single combined dose of 5 mg of antibodies. This dosage is purposely given to elicit a suboptimal level of protection with the cZMAb and MB-003 cocktails, such that potential improvements with the optimized mAb combinations can be identified. Of the tested cocktails, ZMapp1 showed the best protection, with 4 of 6 survivors and less than 5% average weight loss (Table 1). ZMapp2 was next with 3 of 6 survivors and 8% average weight loss, and ZMapp3 protected 1 of 6 animals (Table 1). The level of protection afforded by ZMapp3 was not a statistically significant increase over cZMAb ($P = 0.224$, log-rank test compared to ZMAb, $\chi^2 = 1.479$, degrees of freedom (d.f.) = 1), and showed the same survival rate along with a similar average weight loss (Table 1). As a result, only ZMapp1 and ZMapp2 were carried forward to NHP studies.

ZMapp1 or ZMapp2–treated NHPs

Rhesus macaques were used to determine whether administration of ZMapp1 or ZMapp2 was superior to ZMAb and MB-003 in terms of extending the treatment window. Owing to mAb availability constraints, m4G7 was used in place of c4G7 for this NHP experiment. The experiment consisted of six NHPs per group receiving three doses of ZMapp1 (Group A) or ZMapp2 (Group B) at 50 mg kg^{-1} intravenously at 3-day intervals, beginning 3 days after a lethal intramuscular challenge with 4,000 × median tissue culture infective dose ($TCID_{50}$) (or 2,512 plaque-forming units (p.f.u.)) of EBOV-K. Control animals were given phosphate-buffered saline (PBS) or mAb 4E10 (C1 and C2, respectively). Mock-treated animals succumbed to disease between 6–7 dpi with symptoms typical of EBOV (Fig. 1a), characterized by high clinical scores but no fever (Fig. 1b, c), in addition to viral titres up to approximately 10^8 and 10^9 $TCID_{50}$ by the time of death (Fig. 1d). Analysis of blood counts and serum biochemistry revealed leukocytopenia, thrombocytopenia, severe rash, decreased levels of glucose, as well as increased levels of alkaline phosphatase, alanine aminotransferase, blood urea nitrogen and creatinine at end-stage EBOV disease (Fig. 1e–o, Table 2).

All six Group A NHPs survived the challenge with mild signs of disease (Fig. 1a, Table 2) ($P = 0.0039$, log-rank test, $\chi^2 = 8.333$, d.f. = 1, comparing to Group C), with the exception of A1 which showed an elevated clinical score (Fig. 1b), increased levels of alanine aminotransferase, total bilirubin, and decreased phosphate (Fig. 1, Table 2). However, this animal recovered after the third ZMapp1 dose and the clinical score dropped to zero by 15 dpi (Fig. 1b). A fever was detected in all but one of the NHPs (A4) at 3 dpi, the start of the first ZMapp1 dose (Fig. 1c). Viraemia was also detected beginning at 3 dpi by $TCID_{50}$ in all but one animal from blood sampled just before the administration of treatment (A3) (Fig. 1d), and similar results were observed by quantitative PCR with reverse transcription (RT–qPCR, Extended Data Table 1). The viraemia decreased to undetectable levels by 21 dpi. EBOV shedding was not detected from oral, nasal and rectal swabs by RT–qPCR in any of the Group A animals (Extended Data Tables 2–4).

For Group B, 5 of 6 NHPs survived with B3 succumbing to disease at 9 dpi (Fig. 1a) ($P = 0.0039$, log-rank test, $\chi^2 = 8.333$, d.f. = 1, comparing to Group C). Surviving animals showed only mild signs of disease (Table 2). The moribund animal showed increased clinical scores (Fig. 1b),

Table 2 | Clinical findings of EBOV-infected NHPs from 1 to 27 dpi

Animal ID	Treatment group	Clinical findings					Outcome
		Body temperature	Rash	White blood cells	Platelets	Biochemistry	
A1	50 mg kg^{-1} c13C6+c2G4+m4G7, 3 dpi	Fever (6, 9, 14 dpi)			Thrombocytopenia (6, 9 dpi)	ALT" (9, 14 dpi), TBIL" (9 dpi), PHOS# (6 dpi)	Survived
A2	50 mg kg^{-1} c13C6+c2G4+m4G7, 3 dpi	Fever (3 dpi)		Leukocytosis (3 dpi)		CRE# (14 dpi)	Survived
A3	50 mg kg^{-1} c13C6+c2G4+m4G7, 3 dpi	Fever (3 dpi)		Leukocytosis (3 dpi)	Thrombocytopenia (6 dpi)		Survived
A4	50 mg kg^{-1} c13C6+c2G4+m4G7, 3 dpi			Leukocytopenia (9 dpi)	Thrombocytopenia (3, 6, 14, 21, 27 dpi)		Survived
A5	50 mg kg^{-1} c13C6+c2G4+m4G7, 3 dpi	Fever (3, 6, 9 dpi)		Leukocytopenia (9 dpi)	Thrombocytopenia (3, 21 dpi)		Survived
A6	50 mg kg^{-1} c13C6+c2G4+m4G7, 3 dpi	Fever (3 dpi)					Survived
B1	50 mg kg^{-1} ZMapp2, 3 dpi	Fever (3, 14, 21 dpi)		Leukocytopenia (6, 14, 21, 27 dpi)	Thrombocytopenia (6 dpi)		Survived
B2	50 mg kg^{-1} ZMapp2, 3 dpi	Fever (3, 6 dpi)			Thrombocytopenia (6, 9 dpi)		Survived
B3	50 mg kg^{-1} ZMapp2, 3 dpi	Fever (3, 6 dpi), Hypothermia (9 dpi)	Severe rash (9 dpi)		Thrombocytopenia (6, 9 dpi)	ALT""" (9 dpi), TBIL"" (9 dpi), BUN""" (9 dpi), CRE""" (9 dpi), GLU## (9 dpi)	Died, 9 dpi
B4	50 mg kg^{-1} ZMapp2, 3 dpi	Fever (3, 6 dpi)		Leukocytopenia (6 dpi)	Thrombocytopenia (6, 27 dpi)		Survived
B5	50 mg kg^{-1} ZMapp2, 3 dpi	Fever (3, 6, 14, 21 dpi)		Leukocytosis (3 dpi)	Thrombocytopenia (3, 6 dpi)		Survived
B6	50 mg kg^{-1} ZMapp2, 3 dpi	Fever (3 dpi)		Leukocytosis (3 dpi), Leukocytopenia (6, 9, 14, 21, 27 dpi)	Thrombocytopenia (6 dpi)	PHOS# (3 dpi), CRE# (27 dpi)	Survived
C1	PBS, 3 dpi		Moderate rash (6 dpi), Severe rash (7 dpi)	Leukocytosis (3 dpi)	Thrombocytopenia (6, 7 dpi)	ALB# (7 dpi), ALT" (7 dpi), BUN" (7 dpi)	Died, 7 dpi
C2	Control mAb, 3 dpi		Severe rash (6 dpi)	Leukocytopenia (6, 7 dpi)	Thrombocytopenia (6, 7 dpi)	ALP" (3 dpi), ALT""" (6 dpi), BUN" (6 dpi), CRE""" (6 dpi)	Died, 6 dpi

Hypothermia was defined as below 35 uC. Fever was defined as >1.0 uC higher than baseline. Mild rash was defined as focal areas of petechiae covering <10% of the skin, moderate rash as areas of petechiae covering 10 to 40% of the skin, and severe rash as areas of petechiae and/or ecchymosis covering >40% of the skin. Leukocytopenia and thrombocytopenia were defined as a >30% decrease in numbers of white blood cells and platelets, respectively. Leukocytosis and thrombocytosis were defined as a twofold or greater increase in numbers of white blood cells and platelets over baseline, where white blood cell count > 11 × 10^3. ", two- to threefold increase; "", four- to fivefold increase; """, greater than fivefold increase; #, two- to threefold decrease; ##, four- to fivefold decrease; ###, greater than fivefold decrease. ALB, albumin; ALP, alkaline phosphatase; ALT, alanine aminotransferase; AMY, amylase; TBIL, total bilirubin; BUN, blood urea nitrogen; PHOS, phosphate; CRE, creatinine; GLU, glucose; GLOB, globulin.

in addition to a drastic drop in body temperature shortly before death (Fig. 1c). At the time of death, animal B3 had elevated levels of alanine aminotransferase, total bilirubin, blood urea nitrogen and creatinine, in addition to decreased levels of glucose, suggesting multiple organ failure (Fig. 1). All six Group B animals showed fever in addition to viraemia at 3 dpi by $TCID_{50}$ and RT–qPCR (Fig. 1d, Extended Data Table 1). It was interesting to note that in B3, the viraemia reached approximately 10^6 $TCID_{50}$ after 3 dpi (Fig. 1d), suggesting that this NHP was particularly susceptible to EBOV infection. No escape mutants were detected with this animal. The administration of ZMapp2 at the reported concentrations was unable to effectively control viraemia at this level. Virus shedding was also detected from the oral and rectal swabs by RT–qPCR in the moribund NHP B3 (Extended Data Tables 2–4). Since ZMapp1 demonstrated superior protection to ZMapp2 in this survival study, ZMapp1 (now trademarked as ZMapp by MappBio Pharmaceuticals) was carried forward to test the limits of protection conferred by this mAb cocktail in a subsequent investigation.

ZMapp-treated NHPs

In this experiment, rhesus macaques were assigned into three treatment groups of six and a control group of three animals, with all treatment NHPs receiving three doses of ZMapp (c13C6+c2G4+c4G7, 50 mg kg^{-1} per dose) spaced 3 days apart. After a lethal intramuscular challenge with 1,000 × $TCID_{50}$ (or 628 p.f.u.) of EBOV-K[18], we treated the animals with ZMapp at 3, 6 and 9 dpi (Group D); 4, 7, and 10 dpi (Group E); or 5, 8 and 11 dpi (Group F). The control animals (Group G) were given mAb 4E10 as an IgG isotype control ($n = 1$) or PBS ($n = 2$) in place of ZMapp starting at 4 dpi (Fig. 2a). All animals treated with ZMapp survived the infection, whereas the three control NHPs (G1, G2 and G3) succumbed to EBOV-K infection at 4, 8 and 8 dpi, respectively ($P = 3.58 \times 10^{-5}$, log-rank test, $\chi^2 = 23.25$, d.f. = 3, comparing all groups) (Fig. 2b). At the time ZMapp treatment was initiated, fever, leukocytosis, thrombocytopenia and viraemia could be detected in the majority of the animals (Fig. 2c–f, Table 3, Extended Data Table 5). All animals presented with detectable abnormalities in blood counts and serum biochemistry during the course of the experiment (Fig. 2g–l, Table 3).

The Group F animals did not seem to be as sick as animals E4 and E6 on the basis of clinical scores (Fig. 2c, Extended Data Fig. 1), both animals E4 and E6 were near the clinical limit for IACUC mandated euthanasia at 5 and 7 dpi, respectively. Animal E4 had a flushed face and severe rash on more than 40% of its body surface between 5 and 8 dpi in addition to nasal haemorrhage at 7 dpi, and animal E6 had a flushed face and petechiae on its arms and legs between 7 and 9 dpi, in addition to jaundice between 10 and 14 dpi. This indicates that host genetic factors may have a role in the differential susceptibility of individual NHPs to EBOV-K infections. Fever, leukocytosis, thrombocytopenia and a

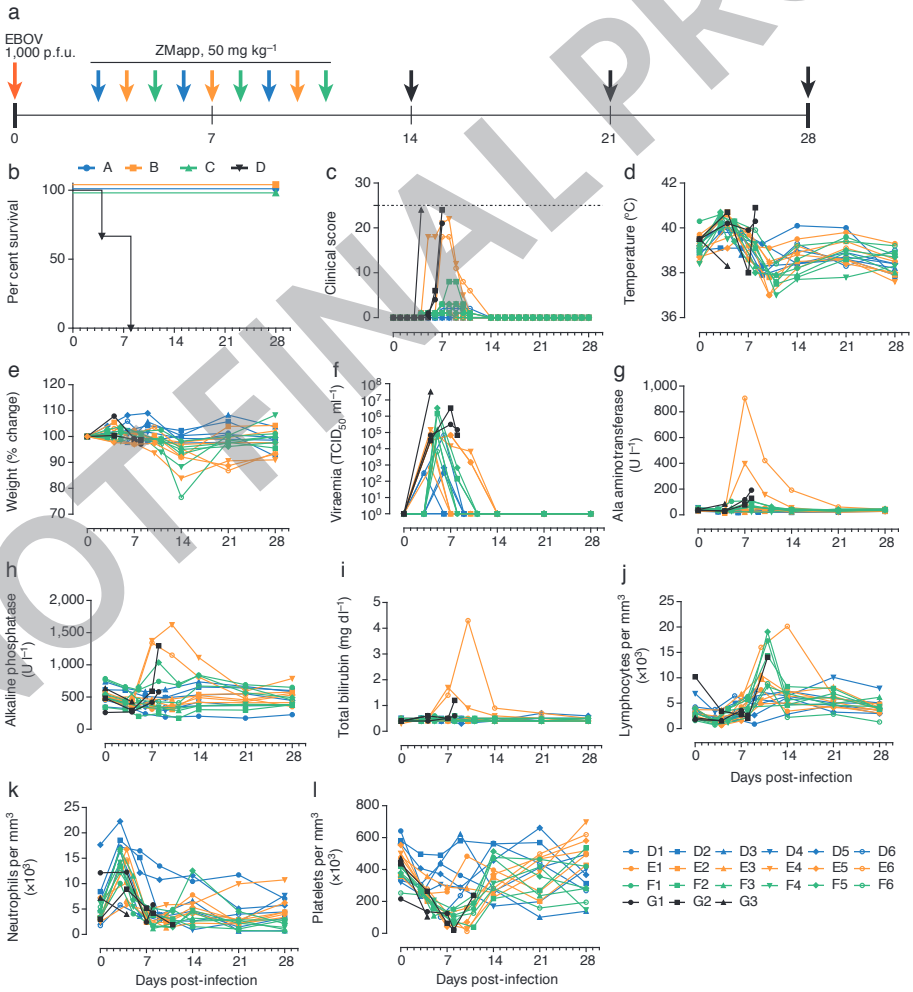

Figure 2 | Post-exposure protection of EBOV-infected nonhuman primates with ZMapp. a–f, Rhesus macaques ($n = 6$ per ZMapp treatment group, $n = 3$ for controls) were challenged with EBOV-K, and 50 mg kg^{-1} of ZMapp were administered beginning at 3 (Group A), 4 (Group B) or 5 (Group C) days after challenge. Non-specific IgG mAb or PBS was administered as a control (Group D). a, Timeline of infection, treatment and sample days. b, Kaplan–Meier survival curves (log-rank test: overall comparison $P = 3.58 \times 10^{-5}$). c, Clinical scores; the dashed line indicates the minimum score requiring mandatory euthanasia. d, Rectal temperature. e, Percentage body weight change. f, EBOV viraemia by $TCID_{50}$. g–l, Selected clinical parameters of Group A to D animals. g, Alanine aminotransferase; h, alkaline phosphatase; i, total bilirubin. j–l, Counts for lymphocytes (j), neutrophils (k) and platelets (l) over the course of the experiment.

Table 3 | Clinical findings of EBOV-infected NHPs from 1 to 28 dpi

Animal ID	Treatment group	Clinical findings					Outcome
		Body temperature	Rash	White blood cells	Platelets	Biochemistry	
D1	50 mg kg^{-1} ZMapp, 3 dpi	Fever (3, 6, 14, 21 dpi)		Leukocytosis (3, 6, 21 dpi)	Thrombocytopenia (3, 6, 9, 14, 21 dpi)	ALB# (14, 21 dpi), ALP# (9, 14, 21, 28 dpi), AMY# (9 dpi), GLOB" (21, 28 dpi)	Survived
D2	50 mg kg^{-1} ZMapp, 3 dpi			Leukocytopenia (21, 28 dpi)	Thrombocytopenia (28 dpi)	PHOS# (9 dpi)	Survived
D3	50 mg kg^{-1} ZMapp, 3 dpi	Fever (3 dpi)		Leukocytosis (3, 14 dpi)	Thrombocytopenia (3, 21, 28 dpi)	ALT# (6 dpi)	Survived
D4	50 mg kg^{-1} ZMapp, 3 dpi			Leukocytopenia (14 dpi)	Thrombocytopenia (14, 21 dpi)	ALT# (9 dpi), CRE" (14 dpi)	Survived
D5	50 mg kg^{-1} ZMapp, 3 dpi	Fever (3 dpi)		Leukocytopenia (21, 28 dpi)	Thrombocytopenia (6, 9 dpi)	ALB# (9 dpi), BUN# (3, 6, 14, 21, 28 dpi)	Survived
D6	50 mg kg^{-1} ZMapp, 3 dpi				Thrombocytopenia (6 dpi)		Survived
E1	50 mg kg^{-1} ZMapp, 4 dpi				Thrombocytopenia (4, 7, 21 dpi)	AMY## (4, 21 dpi), AMY# (7, 10, 14 dpi), CRE# (21, 28 dpi)	Survived
E2	50 mg kg^{-1} ZMapp, 4 dpi	Fever (4 dpi)		Leukocytosis (4, 10 dpi)	Thrombocytopenia (4, 7, 10, 21 dpi)	ALT ## (4 dpi), GLU" (4 dpi)	Survived
E3	50 mg kg^{-1} ZMapp, 4 dpi	Fever (4 dpi)		Leukocytosis (4, 10 dpi)	Thrombocytopenia (7, 10, 14 dpi)	CRE# (14 dpi)	Survived
E4	50 mg kg^{-1} ZMapp, 4 dpi		Severe rash (5, 6, 7, 8 dpi), Mild rash (9 dpi)	Leukocytosis (10, 14, 21, 28 dpi)	Thrombocytopenia (4, 7, 10, 14 dpi)	ALP" (7, 10, 14 dpi), ALT """ (7 dpi), ALT "" (10 dpi), AMY# (4, 7, 10 dpi), TBIL""" (7 dpi), TBIL" (10, 14 dpi), PHOS# (7, 10 dpi), K+# (4 dpi)	Survived
E5	50 mg kg^{-1} ZMapp, 4 dpi	Fever (7 dpi)		Leukocytosis (4 dpi)	Thrombocytopenia (4, 7, 10, 14 dpi)	ALT" (7 dpi), AMY# (4, 7 dpi), PHOS# (10 dpi)	Survived
E6	50 mg kg^{-1} ZMapp, 4 dpi	Fever (4 dpi)	Mild rash (7, 8, 9 dpi)	Leukocytosis (4, 10, 14 dpi)	Thrombocytopenia (4, 7, 10, 14 dpi)	ALP" (7, 10 dpi), ALT """ (7, 10, 14 dpi), AMY# (7, 10 dpi), TBIL"" (7 dpi), TBIL""" (10 dpi), TBIL" (14 dpi), PHOS# (7 dpi), GLOB" (21 dpi)	Survived
F1	50 mg kg^{-1} ZMapp, 5 dpi			Leukocytosis (11 dpi)	Thrombocytopenia (3, 5, 8, 11 dpi)	AMY# (5 dpi), PHOS# (11 dpi), CRE# (28 dpi)	Survived
F2	50 mg kg^{-1} ZMapp, 5 dpi	Fever (3, 5 dpi)	Mild rash (8 dpi)	Leukocytosis (3, 5, 11 dpi)	Thrombocytopenia (3, 5, 8, 11, 14, 21 dpi)	PHOS# (11 dpi), CRE## (11 dpi)	Survived
F3	50 mg kg^{-1} ZMapp, 5 dpi			Leukocytopenia (8 dpi), Leukocytosis (3 dpi)	Thrombocytopenia (5, 8, 11, 21 dpi)	ALT" (8 dpi), CRE## (14 dpi)	Survived
F4	50 mg kg^{-1} ZMapp, 5 dpi	Fever (3, 5 dpi)		Leukocytopenia (8 dpi)	Thrombocytopenia (5, 8, 11, 28 dpi)	PHOS# (8 dpi)	Survived
F5	50 mg kg^{-1} ZMapp, 5 dpi	Fever (3 dpi)		Leukocytosis (3, 11, 14 dpi)	Thrombocytopenia (5, 8, 11 dpi)	PHOS# (5, 8 dpi), CRE# (8, 11, 21, 28 dpi)	Survived
F6	50 mg kg^{-1} ZMapp, 5 dpi	Fever (3 dpi)		Leukocytopenia (8, 21, 28 dpi)	Thrombocytopenia (8, 11, 21 dpi)	PHOS# (5, 8, 11 dpi), GLU" (5 dpi)	Survived
G1	PBS, 4 dpi		Severe rash (4 dpi)	Leukocytopenia (4 dpi)	Thrombocytopenia (4 dpi)	AMY# (4 dpi)	Died, 4 dpi
G2	Control mAb, 4 dpi		Severe rash (8 dpi)	Leukocytopenia (7, 8 dpi)	Thrombocytopenia (4, 7, 8 dpi)	ALP" (8 dpi), ALT" (7 dpi), ALT """ (8 dpi), CRE" (8 dpi)	Died, 8 dpi
G3	PBS, 4 dpi	Fever (4, 8 dpi)	Severe rash (8 dpi)	Leukocytopenia (7, 8 dpi)	Thrombocytopenia (4, 7, 8 dpi)	ALP" (8 dpi), ALT" (7, 8 dpi), AMY# (7 dpi), AMY ## (8 dpi), TBIL" (8 dpi), PHOS# (7 dpi)	Died, 8 dpi

Hypothermia was defined as below 35 uC. Fever was defined as >1.0 uC higher than baseline. Mild rash was defined as focal areas of petechiae covering <10% of the skin, moderate rash was defined as areas of petechiae covering 10 to 40% of the skin, and severe rash was defined as areas of petechiae and/or ecchymosis covering >40% of the skin. Leukocytopenia and thrombocytopenia were defined as a >30% decrease in the numbers of white blood cells and platelets, respectively. Leukocytosis and thrombocytosis were defined as a twofold or greater increase in numbers of white blood cells and platelets above baseline, where white blood cell count > 11×10^3. ", two- to threefold increase; "", four- to fivefold increase; """, greater than fivefold increase; #, two- to threefold decrease; ##, four- to fivefold decrease; ###, greater than fivefold decrease. ALB, albumin; ALP, alkaline phosphatase; ALT, alanine aminotransferase; AMY, amylase; TBIL, total bilirubin; BUN, blood urea nitrogen; PHOS, phosphate; CRE, creatinine; GLU, glucose; K^+, potassium; GLOB, globulin.

severe rash symptomatic of EBOV disease progression were detected in both E4 and E6 (Table 3). Increases in the level of liver enzymes alanine aminotransferase (10- to 30-fold increase), alkaline phosphatase (two- to threefold), and total bilirubin (3- to 11-fold) indicate significant liver damage (Fig. 2g–l), a hallmark of filovirus infections. However, ZMapp was successful in reversing observed disease symptoms and physiological abnormalities after 12 dpi, 2 days after the last ZMapp administration (Table 3). Furthermore, ZMapp treatment was able to lower the high virus loads observed in animals F2 and F5 (up to 10^6 $TCID_{50}$ ml^{-1}) to undetectable levels by 14 dpi (Fig. 2f, Extended Data Fig. 2).

ZMapp cross-reacts with Guinea EBOV

Although the results were very promising with EBOV-K-infected NHPs, it was unknown whether therapy with ZMapp would be similarly effective against the Guinean variant of EBOV (EBOV-G), the virus responsible for the West African outbreak. Direct comparison of published amino acid sequences between EBOV-G and EBOV-K showed that the epitopes targeted by ZMapp[20,21] were not mutated between the two virus variants (Fig. 3a), indicating that the antibodies should retain their specificity for the viral glycoprotein. To confirm this, *in vitro* assays were carried out to compare the binding affinity of c13C6, c2G4 and c4G7 to sucrose-purified EBOV-G and EBOV-K. As measured by enzyme-linked immunosorbent assay (ELISA), the ZMapp components showed slightly better binding kinetics for EBOV-G than for EBOV-K (Fig. 3b). Additionally, the neutralizing activity of individual mAbs was evaluated in the absence of complement for c2G4 and c4G7, and in the presence of complement for c13C6, as they have previously been shown to neutralize EBOV only under these conditions[13] (Fig. 3c). The results supported the ELISA binding data, with comparable neutralizing activities between the two viruses.

Discussion

The West African outbreak of 2014 has highlighted the troubling absence of available vaccine or therapeutic options to save thousands of lives and stop the spread of EBOV. The lack of a clinically acceptable treatment offer limited incentive for people who suspect they might be infected to report themselves for medical help. Several previous studies have showed that antibodies are crucial for host survival from EBOV[22–24]. Prior NHP studies have also demonstrated the ZMAb cocktail could protect 100% or 50% of animals when dosing was initiated 1 or 2 dpi, while the MB-003 cocktail protected 67% of animals with the same dosing regimen. Before the success with monoclonal-antibody-based therapies, other candidate therapeutics had only demonstrated efficacy when given within 60 min of EBOV exposure.

Our results with ZMapp, a cocktail comprising of individual monoclonal antibodies selected from MB-003 and ZMAb, demonstrate for the first time the successful protection of NHPs from EBOV disease when intervention was initiated as late as 5 dpi. In the preceding ZMapp1/ZMapp2 experiment, 11 out of 12 treated animals had detectable fever (with the exception of A4), and live virus could be detected in the blood of 11 out of 12 animals (with the exception of A3) by 3 dpi. Therefore, for the majority of these animals, treatment was therapeutic (as opposed to post-exposure prophylaxis), initiated after two detectable triggers of disease. ZMapp2 was able to protect 5 of 6 animals when administered at 3 dpi. For reasons currently unknown, the lone non-survivor (B3) experienced a viraemia of 10^6 $TCID_{50}$ at 3 dpi, which is 100-fold greater than all other NHPs and approximately tenfold higher than what ZMAb has been reported to suppress in a previous study[16]. This indicates enhanced EBOV replication in this animal, possibly owing to host factors. It is important to note that, despite the high levels of live circulating virus detected in B3, ZMapp2 administration was still able to prolong the life of this animal to 9 dpi, and suggests that in cases of high viraemia such as this, the dosage of monoclonal antibodies should be increased.

The highlight of these experimental results is undoubtedly ZMapp, which was able to reverse severe EBOV disease as indicated by the elevated liver enzymes, mucosal haemorrhages and rash in animals E4 and E6. The high viraemia (up to 10^6 $TCID_{50}$ ml^{-1} of blood in some animals at the time of intervention) could also be effectively controlled without the presence of escape mutants, leading to full recovery of all treated NHPs by 28 dpi. In the absence of direct evidence demonstrating ZMapp efficacy against lethal EBOV-G infection in NHPs, results from ELISA

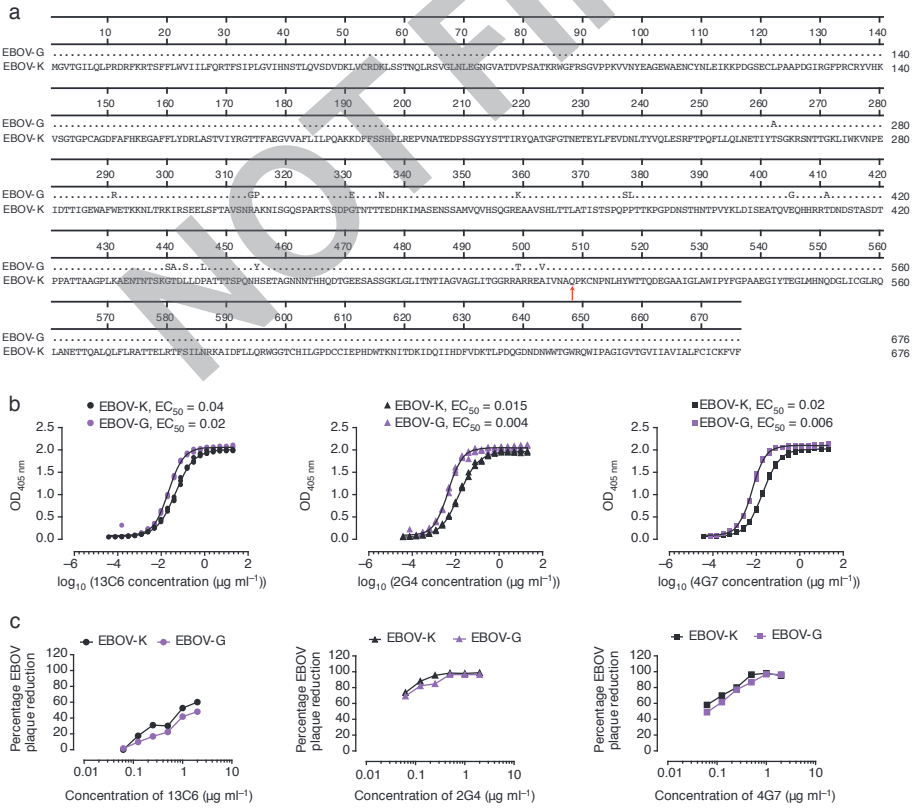

Figure 3 | Amino acid alignment of the Kikwit and Guinea variants of EBOV, and *in vitro* antibody assays of mAbs c13C6, c2G4 and c4G7 with EBOV-G or EBOV-K virions. a, Sequence alignment of the EBOV glycoprotein from the Kikwit (EBOV-K) and Guinea (EBOV-G) variants, with the binding epitopes of ZMapp pointed with an arrow. b, ELISA, not that for each antibody, the median effective concentrations (EC_{50}) are different ($P < 0.05$, regression analysis) between the two antigens. c, Neutralizing antibody assay showing the activity of the individual mAbs composing ZMapp against EBOV-K (black) and EBOV-G (purple), the samples were run in triplicate.

and neutralizing antibody assays show that binding specificity is not abrogated between EBOV-K and EBOV-G, and therefore the levels of protection should not be affected. The compassionate use of ZMapp in two infected American healthcare workers, with apparently positive results pertaining to survival and reversion of EBOV disease[25], may support this assertion. Rhesus macaques have approximately 55–80 ml of blood per kg of body weight[26]; at a dose of 50 mg kg^{-1} of antibodies, the estimated starting concentration is approximately 625–909 μg ml^{-1} of blood (total; , 200–300 μg ml^{-1} for each antibody). Therefore, the low median effective concentration (EC_{50}) values for EBOV-G (0.004–0.02 μg ml^{-1}) bode well for treating EBOV-G infections with ZMapp.

Since the host antibody response is known to correlate with and is required for protection from EBOV infections[23,24], monoclonal-antibody-based treatments are likely to form the centrepiece of any future therapeutic strategies for fighting EBOV outbreaks. However, whether ZMapp-treated survivors can be susceptible to re-infection is unknown. In a previous study of murine ZMAb-treated, EBOV-challenged NHP survivors, a re-challenge of these animals with the same virus at 10 and 13 weeks after initial challenge yielded 6 of 6 survivors and 4 of 6 survivors, respectively[27]. While specific $CD4^+$ and $CD8^+$ T-cell responses could be detected in all animals, the circulating levels of glycoprotein (GP)-specific IgG were shown to be tenfold lower in non-survivors compared to survivors, suggesting that antibody levels may be indicative of protective immunity[27]. Sustained immunity with experimental EBOV vaccines in NHPs remains unknown; however, in a recent study, a decrease in GP-specific IgG levels due to old age or a suboptimal reaction to the VSVΔG/EBOVGP vaccine in rodents also seem to be indicative of non-survival[28].

ZMapp consists of a cocktail of highly purified monoclonal antibodies; which constitutes a less controversial alternative than whole-blood transfusions from convalescent survivors, as was performed during the 1995 EBOV outbreak in Kikwit[29]. The safety of monoclonal antibody therapy is well documented, with generally low rates of adverse reactions, the capacity to confer rapid and specific immunity in all populations, including the young, the elderly and the immunocompromised, and if necessary, the ability to provide higher-than-natural levels of immunity compared to vaccinations[30]. The evidence presented here suggests that ZMapp offers the best option of the experimental therapeutics currently in development for treating EBOV-infected patients. We hope that initial safety testing in humans will be undertaken soon, preferably within the next few months, to enable the compassionate use of ZMapp as soon as possible.

Online Content Methods, along with any additional Extended Data display items and Source Data, are available in the online version of the paper; references unique to these sections appear only in the online paper.

Received 5 August; accepted 21 August 2014.
Published online 29 August 2014.

1. Bausch, D. G., Sprecher, A. G., Jeffs, B. & Boumandouki, P. Treatment of Marburg and Ebola hemorrhagic fevers: a strategy for testing new drugs and vaccines under outbreak conditions. *Antiviral Res.* **78,** 150–161 (2008).
2. Baize, S. *et al.* Emergence of Zaire Ebola virus disease in Guinea — preliminary report. *N. Engl. J. Med.* http://dx.doi.org/10.1056/NEJMoa1404505 (2014).
3. WHO. Ebola virus disease (EVD) http://www.who.int/csr/don/archive/disease/ebola/en/ (accessed, 15 August 2014).
4. CDC. Chronology of Ebola Hemorrhagic Fever Outbreaks, http://www.cdc.gov/vhf/ebola/resources/outbreak-table.html (accessed, 15 August 2014).
5. Reliefweb. W. African Ebola epidemic 'likely to last months': UN http://reliefweb.int/report/guinea/w-african-ebola-epidemic-likely-last-months-un (7 March 2014).
6. Clark, D. V., Jahrling, P. B. & Lawler, J. V. Clinical management of filovirus-infected patients. *Viruses* **4,** 1668–1686 (2012).
7. Guimard, Y. *et al.* Organization of patient care during the Ebola hemorrhagic fever epidemic in Kikwit, Democratic Republic of the Congo, 1995. *J. Infect. Dis.* **179** (Suppl. 1), S268–S273 (1999).
8. Hensley, L. E. *et al.* Recombinant human activated protein C for the postexposure treatment of Ebola hemorrhagic fever. *J. Infect. Dis.* **196** (Suppl 2), S390–S399 (2007).
9. Geisbert, T. W. *et al.* Treatment of Ebola virus infection with a recombinant inhibitor of factor VIIa/tissue factor: a study in rhesus monkeys. *Lancet* **362,** 1953–1958 (2003).
10. Geisbert, T. W. *et al.* Postexposure protection of non-human primates against a lethal Ebola virus challenge with RNA interference: a proof-of-concept study. *Lancet* **375,** 1896–1905 (2010).
11. Warren, T. K. *et al.* Advanced antisense therapies for postexposure protection against lethal filovirus infections. *Nature Med.* **16,** 991–994 (2010).
12. Feldmann, H. *et al.* Effective post-exposure treatment of Ebola infection. *PLoS Pathog.* **3,** e2 (2007).
13. Olinger, G. G., Jr *et al.* Delayed treatment of Ebola virus infection with plant-derived monoclonal antibodies provides protection in rhesus macaques. *Proc. Natl Acad. Sci. USA* **109,** 18030–18035 (2012).
14. Qiu, X. *et al.* Successful treatment of ebola virus-infected cynomolgus macaques with monoclonal antibodies. *Sci. Transl. Med.* **4,** 138ra181 (2012).
15. Pettitt, J. *et al.* Therapeutic intervention of Ebola virus infection in rhesus macaques with the MB-003 monoclonal antibody cocktail. *Sci. Transl. Med.* **5,** 199ra113 (2013).
16. Qiu, X. *et al.* mAbs and Ad-vectored IFN-α therapy rescue Ebola-infected nonhuman primates when administered after the detection of viremia and symptoms. *Sci. Transl. Med.* **5,** 207ra143 (2013).
17. Giritch, A. *et al.* Rapid high-yield expression of full-size IgG antibodies in plants coinfected with noncompeting viral vectors. *Proc. Natl Acad. Sci. USA* **103,** 14701–14706 (2006).
18. Jahrling, P. B. *et al.* Evaluation of immune globulin and recombinant interferon-alpha2b for treatment of experimental Ebola virus infections. *J. Infect. Dis.* **179** (Suppl 1), S224–S234 (1999).
19. Qiu, X. *et al.* Ebola GP-specific monoclonal antibodies protect mice and guinea pigs from lethal Ebola virus infection. *PLoS Negl. Trop. Dis.* **6,** e1575 (2012).
20. Wilson, J. A. *et al.* Epitopes involved in antibody-mediated protection from Ebola virus. *Science* **287,** 1664–1666 (2000).
21. Qiu, X. *et al.* Characterization of Zaire ebolavirus glycoprotein-specific monoclonal antibodies. *Clin. Immunol.* **141,** 218–227 (2011).
22. Dye, J. M. *et al.* Postexposure antibody prophylaxis protects nonhuman primates from filovirus disease. *Proc. Natl Acad. Sci. USA* **109,** 5034–5039 (2012).
23. Wong, G. *et al.* Immune parameters correlate with protection against ebola virus infection in rodents and nonhuman primates. *Sci. Transl. Med.* **4,** 158ra146 (2012).
24. Marzi, A. *et al.* Antibodies are necessary for rVSV/ZEBOV-GP-mediated protection against lethal Ebola virus challenge in nonhuman primates. *Proc. Natl Acad. Sci. USA* **110,** 1893–1898 (2013).
25. ProMEDmail.org. Ebola virus disease - West Africa (117): WHO, Nigeria, Liberia, drug, more. http://www.promedmail.org/direct.php?id=2666073 (6 August 2014).
26. NC3RS. Practical blood sample volumes for laboratory animals, domestic species and non-human primates. http://www.nc3rs.org.uk/bloodsamplingmicrosite/page.asp?id=426 (accessed, 3 August 2014).
27. Qiu, X. *et al.* Sustained protection against Ebola virus infection following treatment of infected nonhuman primates with ZMAb. *Sci. Rep.* **3,** 3365 (2013).
28. Wong, G. *et al.* Immunization with vesicular stomatitis virus vaccine expressing the Ebola glycoprotein provides sustained long-term protection in rodents. *Vaccine* (in the press).
29. Mupapa, K. *et al.* Treatment of Ebola hemorrhagic fever with blood transfusions from convalescent patients. International Scientific and Technical Committee. *J. Infect. Dis.* **179** (Suppl. 1), S18–S23 (1999).
30. UPMChealthsecurity.org. *Next-Generation Monoclonal Antibodies: Challenges and Opportunities* http://www.upmchealthsecurity.org/our-work/pubs_archive/pubs-pdfs/2013/2013-02-04-next-gen-monoclonal-antibodies.pdf (UPMC Center for Biosecurity, 2013).

Acknowledgements The authors thank K. Tierney, A. Grolla, S. Jones, J. Dong and D. Kobasa for their excellent technical assistance, V. Klimyuk and Y. Gleba for access to the magnICON expression system, and H. Steinkellner for access to transgenic *N. benthamiana*. This work was supported by the Defense Threat Reduction Agency (DTRA contract HDTRA1-13-C-0018), the National Institutes of Health (U19AI109762), the Public Health Agency of Canada (PHAC), and a Canadian Safety and Security Program (CSSP) grant to G.P.K. and X.Q. G.W. is the recipient of a Doctoral Research Award from the Canadian Institute for Health Research (CIHR).

Author Contributions X.Q., G.P.K. and L.Z. designed the experiments. X.Q., G.W., J.A., A.B., L.F., J.B.A., H.F., H.W., J.A., J. P., G.G.O. and G.P.K. performed the experiments. X.Q., G.W., J.A., K.W., B.X., J.E.S., L.Z. and G.P.K. wrote the manuscript. E.H., A.J., J.M., K.S., O.B., N.B., C.G., D.K., M.H.P., J.V., K.W. and L.Z. contributed reagents for this study.

Author Information Reprints and permissions information is available at www.nature.com/reprints. The authors declare competing financial interests: details are available in the online version of the paper. Readers are welcome to comment on the online version of the paper. Correspondence and requests for materials should be addressed to G.P.K. (gary.kobinger@phac-aspc.gc.ca) or L.Z. (larry.zeitlin@mappbio.com).

METHODS

Ethics statement. The guinea pig experiment, in addition to the second and third NHP study (ZMapp1, ZMapp2 and ZMapp) were performed at the National Microbiology Laboratory (NML) as described on Animal use document (AUD) #H-13-003, and has been approved by the Animal Care Committee (ACC) at the Canadian Science Center for Human and Animal Health (CSCHAH), in accordance with the guidelines outlined by the Canadian Council on Animal Care (CCAC). The first study with MB-003 in NHPs was performed at United States Army Medical Research Institute of Infectious Diseases (USAMRIID) under an Institutional Animal Care and Use Committee (IACUC) approved protocol in compliance with the Animal Welfare Act, Public Health Service Policy, and other federal statutes and regulations relating to animals and experiments involving animals. The facility where this research was conducted in accredited by The Association for Assessment and Accreditation of Laboratory Animal Care International and adheres to principles stated in the 8th edition of the *Guide for the Care and Use of Laboratory Animals*, National Research Council (2011; http://grants.nih.gov/grants/olaw/Guide-for-the-care-and-use-of-laboratory-animals.pdf).

Monoclonal antibody production. The large-scale production of mAb cocktails cZMAb, MB-003, ZMapp1, ZMapp2 and ZMapp in addition to control mAb 4E10 (anti-HIV) from *N. benthamiana* under GMP conditions was done by Kentucky BioProcessing (Owensboro, KY) as described previously[13,15,31]. The large-scale production of m4G7 was performed by the Biotechnology Research Institute (Montreal, QC) using a previously described protocol[16].

Viruses. The challenge virus used in NHPs was Ebola virus *H.sapiens*-tc/COD/1995/Kikwit-9510621 (EBOV-K) (order *Mononegavirales*, family *Filoviridae*, species *Zaire ebolavirus*; GenBank accession no. AY354458)[18]. Passage three from the original stock was used for the studies at the NML and passage four was used for the study performed at USAMRIID (the NHP study with the individual MB-003 mAbs). Sequencing of 112 clones from the passage three stock virus revealed that the population ratio of 7U:8U in the EBOV GP editing site was 80:20; sequencing for the passage four stock virus was not performed, and therefore the ratio of 7U:8U in the editing site was unknown. The virus used in guinea pig studies was guinea pig-adapted EBOV, Ebola virus VECTOR/*C.porcellus*-lab/COD/1976/Mayinga-GPA (EBOV-M-GPA) (order *Mononegavirales*, family *Filoviridae*, species *Zaire ebolavirus*; GenBank accession number AF272001.1)[32]. The Guinean variant used in IgG ELISA and neutralizing antibody assays was Ebola virus *H.sapiens*-tc/GIN/2014/Gueckedou-C05 (EBOV-G) (order *Mononegavirales*, family *Filoviridae*, species *Zaire ebolavirus*; GenBank accession no. KJ660348.1)[2].

Animals. Outbred 6–8-week-old female Hartley strain guinea pigs (Charles River) were used for these studies. Animals were infected intraperitoneally with 1,000 × LD_{50} of EBOV-M-GPA. The animals were then treated with one dose of ZMAb, MB-003, ZMapp1, ZMapp2, c13C6, h13F6 or c6D8 totalling 5 mg per guinea pig, and monitored every day for 28 days for survival, weight and clinical symptoms. This study was not blinded, and no animals were excluded from the analysis.

For the MB-003 study performed at USAMRIID, thirteen rhesus macaques (*Macaca mulatta*) were obtained from the USAMRIID primate holding facility, ranging from 5.1 to 10 kg. This study was not blinded, and no animals were excluded from the analysis. Animals were given standard monkey chow, primate treats, fruits, and vegetables for the duration of the study. All animals were challenged intramuscularly with a target dose of 1,000 p.f.u. Treatment with either monoclonal antibody, MB-003 cocktail, or PBS was administered on 1, 4, and 7 dpi via saphenous intravenous infusion. Animals were monitored at least once daily for changes in health, diet, behaviour, and appearance. Animals were sampled for chemical analysis, complete bloods counts and viraemia on 0, 3, 5, 7, 10, 14, 21, and 28 dpi.

For the ZMapp1 and ZMapp2 study, fourteen male and female rhesus macaques (*Macaca mulatta*), ranging from 4.1 to 9.6 kg (4–8 years old) were purchased from Primgen (USA). This study was not blinded, and no animals were excluded from the analysis. Animals were assigned groups based on gender and weight. Animals were fed standard monkey chow, fruits, vegetables, and treats. Husbandry enrichment consisted of visual stimulation and commercial toys. All animals were challenged intramuscularly with a high dose of EBOV (backtitre: 4,000 × $TCID_{50}$ or 2,512 p.f.u.] at 0 dpi. Administration of the first treatment dose was initiated at 3 dpi, with identical doses at 6 and 9 dpi. Animals were scored daily for signs of disease, in addition to changes in food and water consumption. On designated treatment days in addition to 14, 21, and 27 dpi, the rectal temperature and clinical score were measured, and the following were sampled: blood for serum biochemistry and cell counts and viraemia. This study was not blinded, and no animals were excluded from the analysis.

For the ZMapp study, twenty-one male rhesus macaques, ranging from 2.5 to 3.5 kg (2 years old) were purchased from Primgen (USA). This study was not blinded, and no animals were excluded from the analysis. Animals were assigned groups based on gender and weight. Animals were fed standard monkey chow, fruits, vegetables, and treats. Husbandry enrichment consisted of visual stimulation and commercial toys. All animals were challenged intramuscularly with EBOV (backtitre: 1,000 × $TCID_{50}$ or 628 p.f.u.] at 0 dpi. Administration of the first treatment dose was initiated at 3, 4 or 5 dpi, with two additional identical doses spaced 3 days apart. Animals were scored daily for signs of disease, in addition to changes in food and water consumption. On designated treatment days in addition to 14, 21, and 28 dpi, the rectal temperature and clinical score were measured, and the following were sampled: blood for serum biochemistry and cell counts and viraemia.

Blood counts and blood biochemistry. Complete blood counts were performed with the VetScan HM5 (Abaxis Veterinary Diagnostics). The following parameters were shown in the figures: levels of white blood cells, lymphocytes, percentage of lymphocytes, levels of platelets, neutrophils and percentage of neutrophils. Blood biochemistry was performed with the VetScan VS2 (Abaxis Veterinary Diagnostics). The following parameters were shown in the figures: levels of alkaline phosphatase, alanine aminotransferase, blood urea nitrogen, creatinine, and total bilirubin.

Enzyme-linked immunosorbent assays (ELISAs). IgG ELISA with c13C6, c2G4 or c1H3 was performed as described previously[16] using gamma-irradiated EBOV-G and EBOV-K virions purified on a 20% sucrose cushion as the capture antigen in the ELISA. Each mAb was assayed in triplicate.

Neutralizing antibody assays. Twofold dilutions of c13C6, c2G4 or c1H3 ranging from 0.0156 to 2 mg were first incubated with 100 p.f.u. of EBOV-G at room temperature for 1 h with or without complement, transferred to Vero E6 cells and incubated at 37 uC for 1 h, and then replaced with DMEM supplemented with 2% fetal bovine serum and scored for the presence of cytopathic effect at 14 dpi. The lowest concentrations of mAbs demonstrating the absence of cytopathic effect were averaged and reported.

EBOV titration by $TCID_{50}$ and RT–qPCR. Titration of live EBOV was determined by adding tenfold serial dilutions of whole blood to VeroE6 cells, with three replicates per dilution. The plates were scored for cytopathic effect at 14 dpi, and titres were calculated with the Reed and Muench method[33]. Results were shown as median tissue culture infectious dose ($TCID_{50}$).

For titres measured by RT–qPCR, total RNA was extracted from whole blood with the QIAmp Viral RNA Mini Kit (Qiagen). EBOV was detected with the LightCycler 480 RNA Master Hydrolysis Probes (Roche) kit, with the RNA polymerase (nucleotides 16472 to 16538, AF086833) as the target gene. The reaction conditions were as follows: 63 uC for 3 min, 95 uC for 30 s, and cycling of 95 uC for 15 s, 60 uC for 30 s for 45 cycles on the ABI StepOnePlus. The lower detection limit for this assay is 86 genome equivalents ml^{-1}. The sequences of primers used were as follows: EBOVLF2 (CAGCCAGCAATTTCTTCCAT), EBOVLR2 (TTTCGGTTGCTGTTTCTGTG), and EBOVLP2FAM (FAM-ATCATTGGCGTACTGGAGGAGCAG-BHQ1).

Sequence alignment. Protein sequences for EBOV-K and EBOV-G surface glycoproteins were obtained from GenBank, accession numbers AGB56794.1 and AHX24667.1 respectively. The sequences were aligned using DNASTAR Lasergene 10 MEGAlign using the Clustal W algorithm.

Statistical analysis. For the guinea pig and nonhuman primate studies, each treatment group consisted of six animals. Assuming a significance threshold of 0.05, a sample size of six per group will give >80% power to detect a difference in survival proportions between the treatment (83% survival or higher) and the control group using a one-tailed Fisher's exact test.

Survival was compared using the log-rank test in GraphPad PRISM 5, differences in survival were considered significant when the *P* value was less than 0.05. Antibody binding to EBOV-G and EBOV-K was compared by fitting the data to a four-parameter logistic regression using GraphPad PRISM 5. The EC_{50} were considered different if the 95% confidence intervals excluded each other. For all statistical analyses, the data conformed to the assumptions of the test used.

31. Zeitlin, L. *et al.* Enhanced potency of a fucose-free monoclonal antibody being developed as an Ebola virus immunoprotectant. *Proc. Natl Acad. Sci. USA* **108,** 20690–20694 (2011).
32. Connolly, B. M. *et al.* Pathogenesis of experimental Ebola virus infection in guinea pigs. *J. Infect. Dis.* **179** (Suppl. 1), S203–S217 (1999).
33. Reed, L. J. & Muench, H. A simple method of estimating fifty per cent endpoints. *Am. J. Hyg.* **27,** 493–497 (1938).

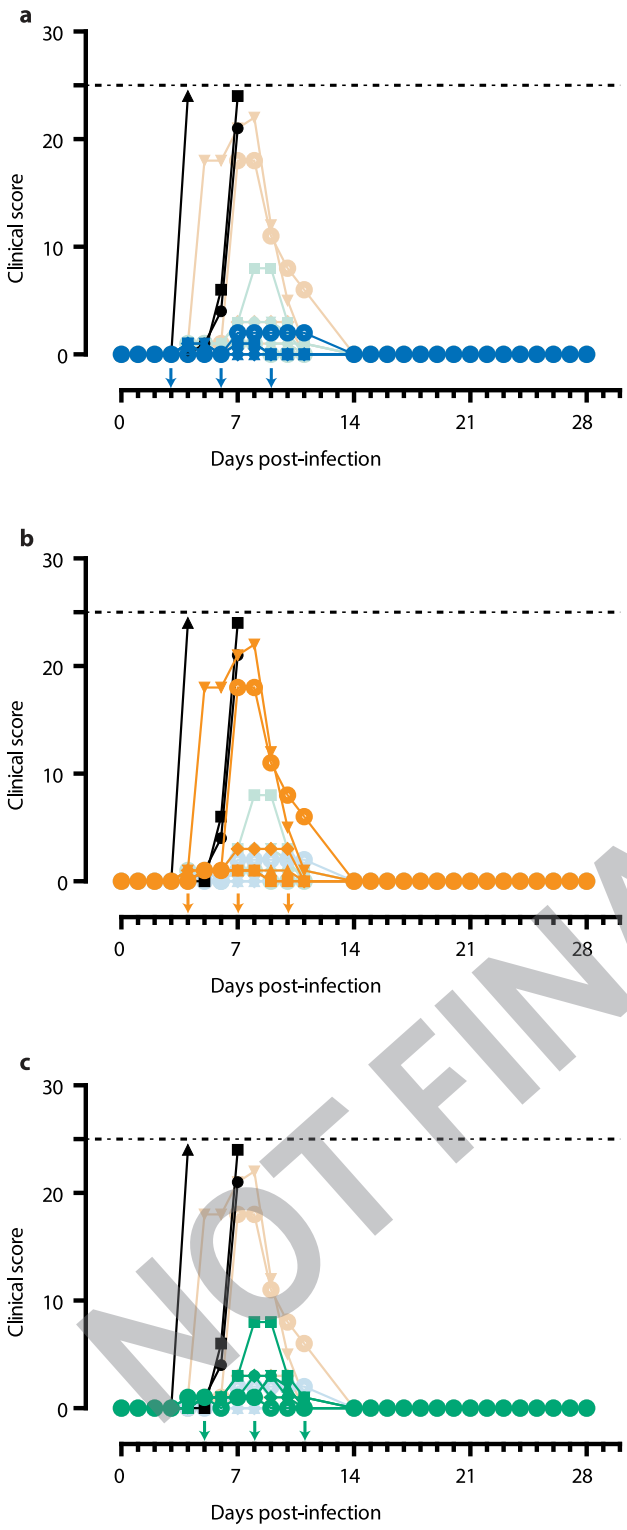

Extended Data Figure 1 | Clinical scores for each ZMapp-treated group. Arrows indicate treatment days. Dashed line represents humane endpoint threshold. Faded symbols/lines are the other two treatment groups, for comparison. Control group (Group G) is shown in black on all three panels. a, Clinical score of Group D (blue); b, clinical score of Group E (orange); c, clinical score of Group F (green).

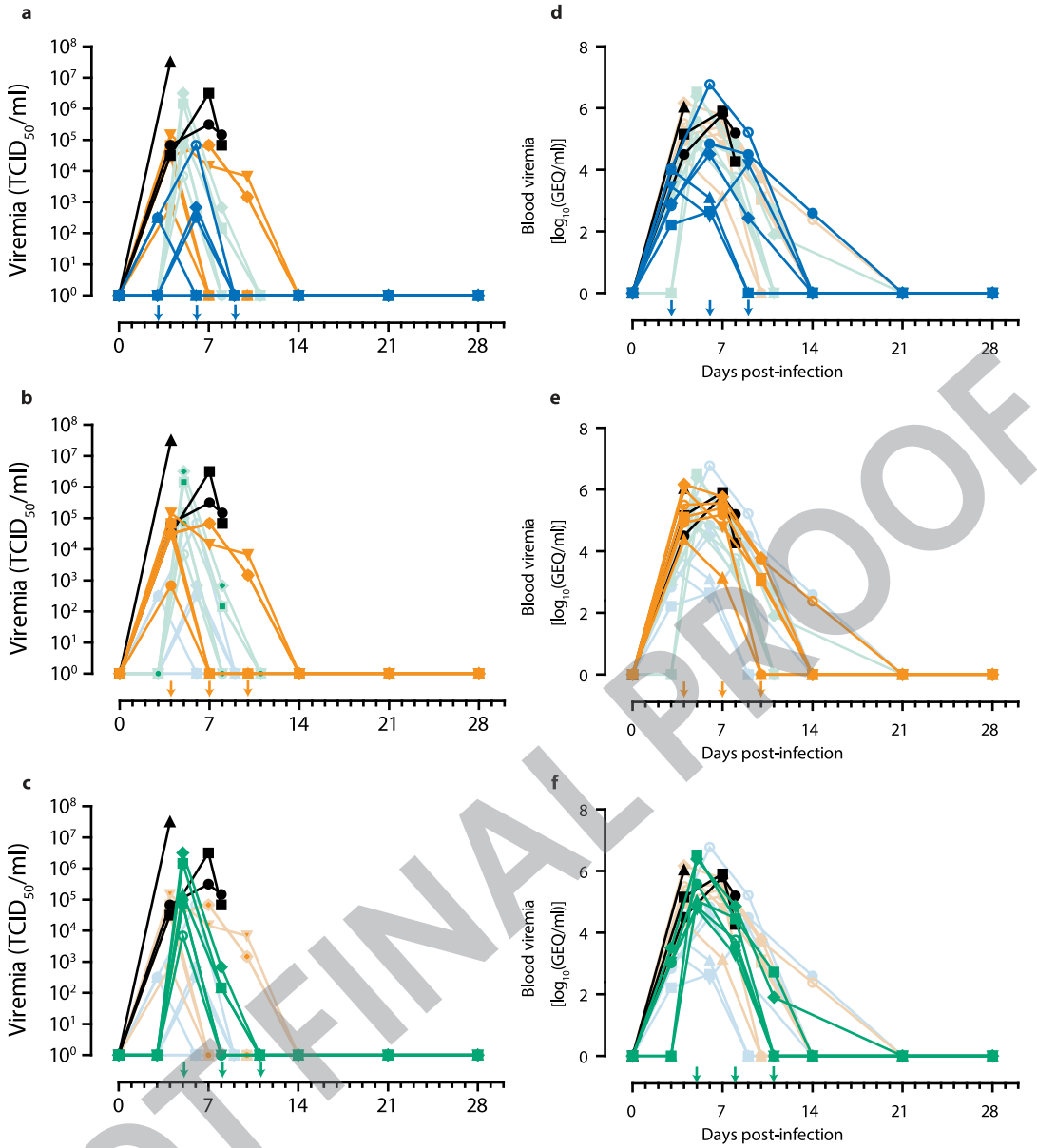

Extended Data Figure 2 | Viraemia for each ZMapp-treated group. Arrows indicate treatment days. Faded symbols/lines are the other two treatment groups, for comparison. Control group (Group G) is shown in black on all three panels. a, $TCID_{50}$ of Group D (blue); b, $TCID_{50}$ of Group E (orange); c, $TCID_{50}$ of Group F (green). d, Viraemia by RT–qPCR of Group D (blue); e, Viraemia by RT–qPCR of Group E (orange); f, Viraemia by RT–qPCR of Group F (green).

Extended Data Table 1 | Blood viraemia measured by RT–qPCR for the ZMapp1- and ZMapp2-treated NHPs

Day	A1	A2	A3	A4	A5	A6	B1	B2	B3	B4	B5	B6	C1	C2
0	UD	UD	UD	UD	UD	UD	UD	UD	UD	UD	UD	UD	UD	UD
3	UD	3.98E+02	UD	UD	9.99E+02	1.27E+03	8.05E+03	1.65E+04	9.36E+03	9.77E+03	9.27E+02	9.48E+02	UD	4.34E+02
6	3.10E+03	4.49E+02	UD	8.34E+02	5.81E+03	2.09E+03	UD	1.22E+04	1.04E+05	4.26E+03	3.14E+02	4.49E+03	5.57E+06	2.05E+07
7													5.50E+05	
9		UD	UD	UD	UD	5.24E+02	UD	1.74E+05	5.03E+05	1.87E+03	5.16E+02	UD		
14	3.62E+03	UD	UD	UD	UD	UD	UD	UD		UD	UD	UD		
21	UD	UD	UD	UD	UD	UD	UD	UD		UD	UD	UD		
27	UD	UD	UD	UD	UD	UD	UD	UD		UD	UD	UD		

UD, undetectable.

Extended Data Table 2 | Oral swab viraemia measured by RT–qPCR for the ZMapp1- and ZMapp2-treated NHPs

Days	A1	A2	A3	A4	A5	A6	B1	B2	B3	B4	B5	B6	C1	C2
0	UD	UD	UD	UD	UD	UD	UD	UD	UD	UD	UD	UD	UD	UD
3	UD	UD	UD	UD	UD	UD	UD	UD	UD	UD	UD	UD	UD	UD
6	UD	UD	UD	UD	UD	UD	UD	UD	UD	UD	UD	UD	UD	UD
7													5.05E+03	
9		UD	UD	UD	UD	UD	UD	UD	4.81E+04	UD	UD	UD		
14	UD	UD	UD	UD	UD	UD	UD	UD		UD	UD	UD		
21	UD	UD	UD	UD	UD	UD	UD	UD		UD	UD	UD		
27	UD	UD	UD	UD	UD	UD	UD	UD		UD	UD	UD		

UD, undetectable.

Extended Data Table 3 | Nasal swab viraemia measured by RT–qPCR for the ZMapp1- and ZMapp2-treated NHPs

Days	A1	A2	A3	A4	A5	A6	B1	B2	B3	B4	B5	B6	C1	C2
0	UD	UD	UD	UD	UD	UD	UD	UD	UD	UD	UD	UD	UD	UD
3	UD	UD	UD	UD	UD	UD	UD	UD	UD	UD	UD	UD	UD	UD
6	UD	UD	UD	UD	UD	UD	UD	UD	UD	UD	UD	UD	UD	3.75E+02
7													1.98E+04	2.16E+03
9		UD	UD	UD	UD	UD	UD	UD	UD	UD	UD	UD		
14	UD	UD	UD	UD	UD	UD	UD	UD		UD	UD	UD		
21	UD	UD	UD	UD	UD	UD	UD	UD		UD	UD	UD		
27	UD	UD	UD	UD	UD	UD	UD	UD		UD	UD	UD		

UD, undetectable.

Extended Data Table 4 | Rectal swab viraemia measured by RT–qPCR for the ZMapp1- and ZMapp2-treated NHPs

Days	A1	A2	A3	A4	A5	A6	B1	B2	B3	B4	B5	B6	C1	C2
0	UD	UD	UD	UD	UD	UD	UD	UD	UD	UD	UD	UD	UD	UD
3	UD	UD	UD	UD	UD	UD	UD	UD	UD	UD	UD	UD	UD	UD
6	UD	UD	UD	UD	UD	UD	UD	UD	UD	UD	UD	UD	4.16E+02	8.17E+03
7													4.38E+04	
9		UD	UD	UD	UD	UD	UD	UD	3.90E+02	UD	UD	UD		
14	UD	UD	UD	UD	UD	UD	UD	UD		UD	UD	UD		
21	UD	UD	UD	UD	UD	UD	UD	UD		UD	UD	UD		
27	UD	UD	UD	UD	UD	UD	UD	UD		UD	UD	UD		

UD, undetectable.

Extended Data Table 5 | Blood viraemia measured by RT–qPCR for the ZMapp-treated NHPs

Days	A1	A2	A3	A4	A5	A6	B1	B2	B3	B4	B5	B6	C1	C2	C3	C4	C5	C6	D1	D2	D3
0	1	1	1	1	1	1	1	1	1	1	1	1	1	1	1	1	1	1	1	1	1
3	676.08	165.96	10233	2884	812.83	10965							1047.1			1122	3235.9	1148.2			
4							85114	128825	23442	1E+06	1E+06	323594							31623	144544	1E+06
5													380189	3E+06	109648	58884	2E+06	69183			
6	70795	446.68	1230.3	316.23	32359	6E+06															
7							154882	257040	1380.4	63096	588844	363078							645654	812831	
8													3715.4	28184	29512	1862.1	72444	5888.4	158489	18621	
9	31623	1	1	15136	275.42	165959															
10							1	1071.5	1	1318.3	6166	5248.1									
11													1	524.81	1	1	81.283	1			
14	398.11	1	1	1	1	1	1	1	1	1	1	239.88	1	1	1	1	1	1			
21	1	1	1	1	1	1	1	1	1	1	1	1	1	1	1	1	1	1			
28	1	1	1	1	1	1	1	1	1	1	1	1	1	1	1	1	1	1			

CellPress

Molecular Cell
Article

Assessing the ceRNA Hypothesis with Quantitative Measurements of miRNA and Target Abundance

Rémy Denzler,[1,2] Vikram Agarwal,[3,4,5] Joanna Stefano,[3,4] David P. Bartel,[3,4,*] and Markus Stoffel[1,2,*]
[1]Institute of Molecular Health Sciences, ETH Zurich, Otto-Stern-Weg 7, HPL H36, 8093 Zurich, Switzerland
[2]Competence Center of Systems Physiology and Metabolic Disease, ETH Zurich, Otto-Stern-Weg 7, 8093 Zurich, Switzerland
[3]Howard Hughes Medical Institute and Whitehead Institute for Biomedical Research, Cambridge, MA 02142, USA
[4]Department of Biology, Massachusetts Institute of Technology, Cambridge, MA 02139, USA
[5]Computational and Systems Biology Program, Massachusetts Institute of Technology, Cambridge, MA 02139, USA
*Correspondence: dbartel@wi.mit.edu (D.P.B.), stoffel@biol.ethz.ch (M.S.)
http://dx.doi.org/10.1016/j.molcel.2014.03.045

SUMMARY

Recent studies have reported that competitive endogenous RNAs (ceRNAs) can act as sponges for a microRNA (miRNA) through their binding sites and that changes in ceRNA abundances from individual genes can modulate the activity of miRNAs. Consideration of this hypothesis would benefit from knowing the quantitative relationship between a miRNA and its endogenous target sites. Here, we altered intracellular target site abundance through expression of an miR-122 target in hepatocytes and livers and analyzed the effects on miR-122 target genes. Target repression was released in a threshold-like manner at high target site abundance ($\geq$1.5 × 10^5 added target sites per cell), and this threshold was insensitive to the effective levels of the miRNA. Furthermore, in response to extreme metabolic liver disease models, global target site abundance of hepatocytes did not change sufficiently to affect miRNA-mediated repression. Thus, modulation of miRNA target abundance is unlikely to cause significant effects on gene expression and metabolism through a ceRNA effect.

INTRODUCTION

MicroRNAs (miRNAs) are an abundant class of small noncoding RNAs that regulate gene expression at the levels of mRNA stability and translation (Pillai et al., 2005; Eulalio et al., 2008; Guo et al., 2010). They pair to target sites (referred to as miRNA response elements [MREs]) within mRNAs to direct the posttranscriptional downregulation of these mRNA targets. The human genome has more than 500 miRNA genes, and miRNAs from individual gene families are able to target hundreds of different messenger RNAs (Baek et al., 2008; Friedman et al., 2009). Given that more than half of all human mRNAs are estimated to be conserved miRNA targets, miRNAs are thought to have widespread effects on gene regulation (Friedman et al., 2009). Even though many miRNA knockout models show no apparent defect under normal conditions, they frequently exhibit miRNA-dependent phenotypes when specific stresses are applied (Li et al., 2009; Brenner et al., 2010). Therefore, miRNAs are proposed to be critical regulators in stress signal mediation and modulation, where inadequate miRNA levels and responses can cause or exacerbate disease (Mendell and Olson, 2012).

Highly expressed site-containing RNAs, either found naturally or delivered as research reagents, can act as "sponges" to titrate miRNAs away from other normal targets (Ebert et al., 2007; Franco-Zorrilla et al., 2007; Mukherji et al., 2011; Hansen et al., 2013; Memczak et al., 2013). Theoretical and experimental reports have claimed that crosstalk between site-containing RNAs extends far beyond a few highly expressed sponges. Analyses of high-throughput data sets indicate that the activity of a miRNA is not just dependent on its levels but also its relative target site abundance (TA), defined as the relative number of sites within the transcriptome for that miRNA (Arvey et al., 2010; Garcia et al., 2011). One hypothesis suggests that this crosstalk has a widespread regulatory function, with the act of titrating miRNAs away from their other targets somehow explaining why so many target sites have been conserved in evolution (Seitz, 2009). This idea is extended to the notion that many miRNA targets act as competitive endogenous RNAs (ceRNAs) that modulate the repression of other targets as their expression increases or decreases (Salmena et al., 2011; Tay et al., 2011). Experimental evidence for such a ceRNA crosstalk was initially described for the tumor-suppressor gene *PTEN*, which appears to be regulated by the abundance of its pseudogene (*PTENP1*) in a DICER-dependent manner (Poliseno et al., 2010). Recent studies have reported the potential physiological relevance of other ceRNAs, including a long noncoding RNA that regulates muscle differentiation (Cesana et al., 2011), an overexpressed 3′ untranslated region (3′ UTR) inducing cancer in transgenic mice (Fang et al., 2013), and a circular RNA (circRNAs) regulating miR-7 activity in the CNS (Hansen et al., 2013; Memczak et al., 2013). However, such studies have used cancer cell lines with abnormal miRNA and ceRNA expression (Poliseno et al., 2010; Karreth et al., 2011), leaving their physiological relevance in primary cells unclear.

The ceRNA hypothesis is controversial because it is difficult to imagine how the change in expression of individual miRNA targets, which each typically contribute a miniscule fraction of the TA, could possibly influence enough miRNA molecules to affect

regulation of other targets. Consideration of the ceRNA hypothesis would clearly benefit from quantitative knowledge of the intracellular relationship of miRNAs and their corresponding target sites. Although some attempts have been undertaken to evaluate this relationship, the data were typically acquired in silico (Ala et al., 2013; Figliuzzi et al., 2013), in vitro with purified components (Wee et al., 2012), or in experimental setups in which rapidly dividing cells were transfected with synthetic miRNAs, which complicate any interpretations more quantitative than relative comparisons (Arvey et al., 2010; Garcia et al., 2011; Tay et al., 2011). A more recent study not subject to these limitations reported that miRNA efficacy tended to be higher for miRNAs with lower predicted target:miRNA ratios but did not address the question of how much change in ceRNA might be required to detectably influence miRNA efficacy (Mullokandov et al., 2012).

In this study, we analyzed the stoichiometric relationship of miR-122 and its target sites by manipulating TA through controlled expression of a validated target of miR-122 in primary hepatocytes and livers. miR-122 has been linked to important human diseases, such as hepatitis C, liver cancer, and hypercholesterolemia, and its target genes have been well characterized (Jopling et al., 2005; Krützfeldt et al., 2005; Esau et al., 2006; Tsai et al., 2009). Our absolute quantification of relevant entities in primary cells and disease states provided insights on the relationship between miR-122 TA and miR-122 activity. These results will facilitate future studies predicting the biologically relevant range of TAs of other miRNAs and the magnitude of change in target abundance required to influence gene expression through a ceRNA mechanism.

RESULTS

miRNA Target Derepression Is Detected at a High Threshold of Added MREs

To assess the relationship between a miRNA and its MREs and the effect of this relationship on target gene regulation, we chose the highly expressed liver-specific miR-122 as a model system. We manipulated endogenous MREs in a controlled manner by overexpressing a full-length AldolaseA (*AldoA*) mRNA, a strong and validated target of miR-122 (Krützfeldt et al., 2005), using recombinant adenoviruses (Ad-AldoA) carrying either a mutated (Mut), one (1s), or three (3s) miR-122 binding site(s) (Figures 1A and S1A). To eliminate potential off-target effects mediated by the AldoA protein, we introduced a premature stop codon that prevented translation of AldoA protein (Figure S1B).

To assess the stoichiometric relationship of miR-122 and the added MREs in primary hepatocytes, we measured the absolute number of these entities per cell. Quantitative RT-PCR measurements calibrated with an internal standard curve of synthetic miRNA revealed that miR-122 was expressed at 1.2×10^5 molecules per cell (Figure 1B), which was comparable to levels previously reported (Bissels et al., 2009). As expected, miR-16 and miR-33 were each expressed at fewer copies per cell (1.1×10^4 and 1.2×10^3, respectively). Next, we measured the increased miR-122 target abundance after infecting hepatocytes with Ad-AldoA at three different multiplicities of infection (MOI; 2, 20, and 200) with our constructs that introduced zero, one, or three miR-122 MREs per *AldoA* transcript. Adenovirus constructs showed very high transduction efficiencies (Figure S2A), and a linear correlation was observed between viral dose and green fluorescent protein (*GFP*) mRNA, which was expressed from an independent promoter in the Ad-AldoA vector (Figure 1C). Similar results were observed when monitoring GFP protein levels (Figures S2B and S2C). At MOI 200, *AldoA* transcripts increased from 3.3×10^3 (endogenous levels) to $0.8–1.1 \times 10^6$ molecules per cell (Figure 1D), introducing up to 2.6×10^6 *AldoA* MREs per cell (Figure 1E). The ratio of *AldoA* to *GFP* mRNA showed that the *AldoA* transcripts were repressed in an MRE-dependent manner at MOI 2 and 20, which confirmed that miR-122 was functionally engaging the MREs within these transcripts (Figure 1F). This regulation disappeared at MOI 200, suggesting that, at this very high MOI, *AldoA* transcript overwhelmed the regulatory capacity of miR-122 (Figure 1F). Quantification of miR-122 confirmed that the loss of regulation was not due to a loss in miR-122; even at very high levels, Ad-AldoA did not influence the levels of either miR-122 or two control miRNAs, although it did reduce miR-33 by 2-fold (Figure 1G).

Having observed a loss in *AldoA* repression at a high MOI, we reasoned that high levels of *AldoA* transcript could act as a sponge to also derepress cellular miR-122 targets. Indeed, known miR-122 targets, but not a control transcript *ApoM*, increased at a high MOI (Figures 1H and S2D). Interestingly, this derepression was confidently detected only when *AldoA* MREs exceeded $1.5–2.7 \times 10^5$ per cell. This threshold corresponded to 1.25–2.25 MREs per miR-122 molecule. Once this threshold was exceeded, additional *AldoA* MREs led to greater miR-122 target derepression, and the magnitude correlated with the number of miR-122 sites introduced by *AldoA* transcripts. Altogether, these data demonstrate that derepression mediated through increased expression of a miR-122 target can occur but can be detected only after exceeding a high threshold of added MREs.

The High Threshold Persists after Lowering miR-122 Activity

Two scenarios might explain the high threshold of added MREs required to observe endogenous target derepression. The "excess miRNA" scenario posits that very abundant miRNAs are present in excess over their targets, and thus competing MREs would need to titrate this excess binding capacity before they could exert an observable effect on endogenous target repression. Our case of miR-122 in hepatocytes would be one of the more attractive candidates for this scenario, given that miR-122 is the most abundant miRNA in hepatocytes (Landgraf et al., 2007). Indeed, its abundance of 1.2×10^5 molecules per cell is among the highest reported for a miRNA in any mammalian system. The second scenario is the "high TA" scenario. In this scenario, the effective number of miRNA binding sites within cellular transcripts is so high that even highly expressed miRNAs are mostly bound to a site at any moment in time, and thus the number of competing MREs would need to approach this high effective number of sites before the competing MREs could exert an observable impact on endogenous target repression. The idea of many miRNA binding sites within cellular transcripts is supported by reports that many miRNAs have hundreds of

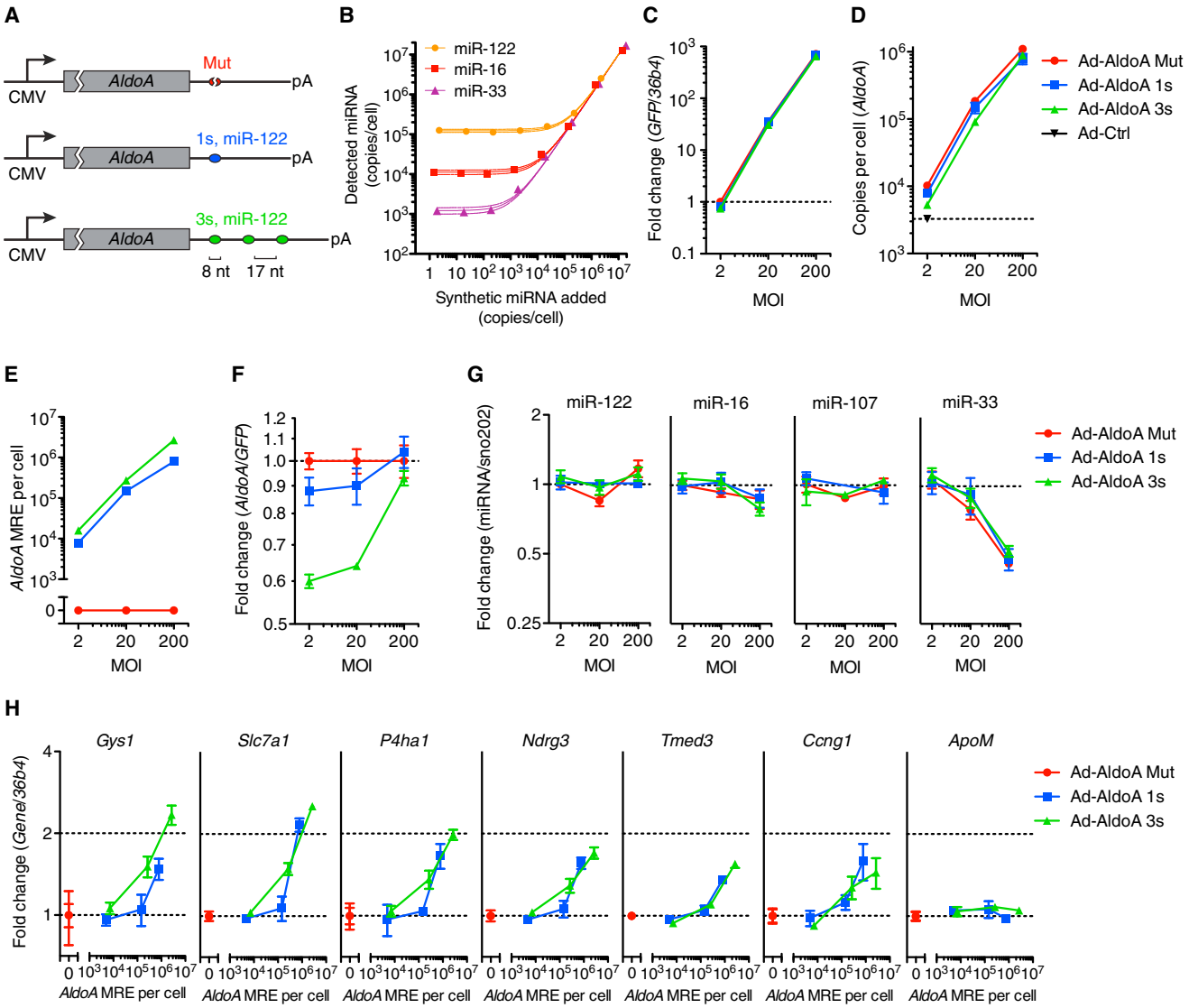

Figure 1. miRNA Target Derepression Is Detected at a High Threshold of Added MREs

(A) Schematic overview of the different *AldoA*-expressing adenovirus constructs (Ad-AldoA) harboring either one (1s, blue) or three (3s, green) miR-122 binding sites or a mutated site (Mut, red). Ad-AldoA 3s contained three 8 nt seed matches of miR-122 separated by 17 nt spacers. See also Figure S1.

(B) Absolute miRNA quantification of primary hepatocyte cell lysates spiked with different amounts of synthetic miRNA. Solid lines represent linear regression data with respective 95% confidence intervals.

(C–H) Primary hepatocytes infected with different multiplicities of infection (MOI) of the Ad-AldoA constructs. Relative gene expression of *GFP* (C) and *AldoA* (F) and absolute copy numbers per cell of *AldoA* (D) and *AldoA* MRE (E). Relative expression of miRNAs (G) or miR-122 target genes and a control nontarget gene (*ApoM*) (H). See also Figure S2.

GFP and miRNA expression are relative to Ad-AldoA Mut at MOI 2; *AldoA*, miR-122 target genes and the control gene are relative to the respective Ad-AldoA Mut at given MOI. Data represent mean ± SEM (n = 3) for all panels.

conserved MREs (Friedman et al., 2009), miRNAs also repress many additional mRNAs with nonconserved MREs (Farh et al., 2005; Krützfeldt et al., 2005; Giraldez et al., 2006; Baek et al., 2008), and high-throughput crosslinking identifies many additional binding sites that would not be classified as MREs because they don't mediate detectable repression (including many sites within open reading frames and marginally effective sites elsewhere) but would nonetheless add to the effective number of binding sites (Hafner et al., 2010). These two scenarios predict two very different responses to miRNA reduction. In the excess miRNA scenario, miRNA reduction would lower the excess miRNA capacity and thereby lower the threshold of added MREs required to observe endogenous target derepression. In the high TA scenario, the effective number of sites already exceeds the miRNA abundance, and, more importantly, the threshold relates to the effective number of binding sites and

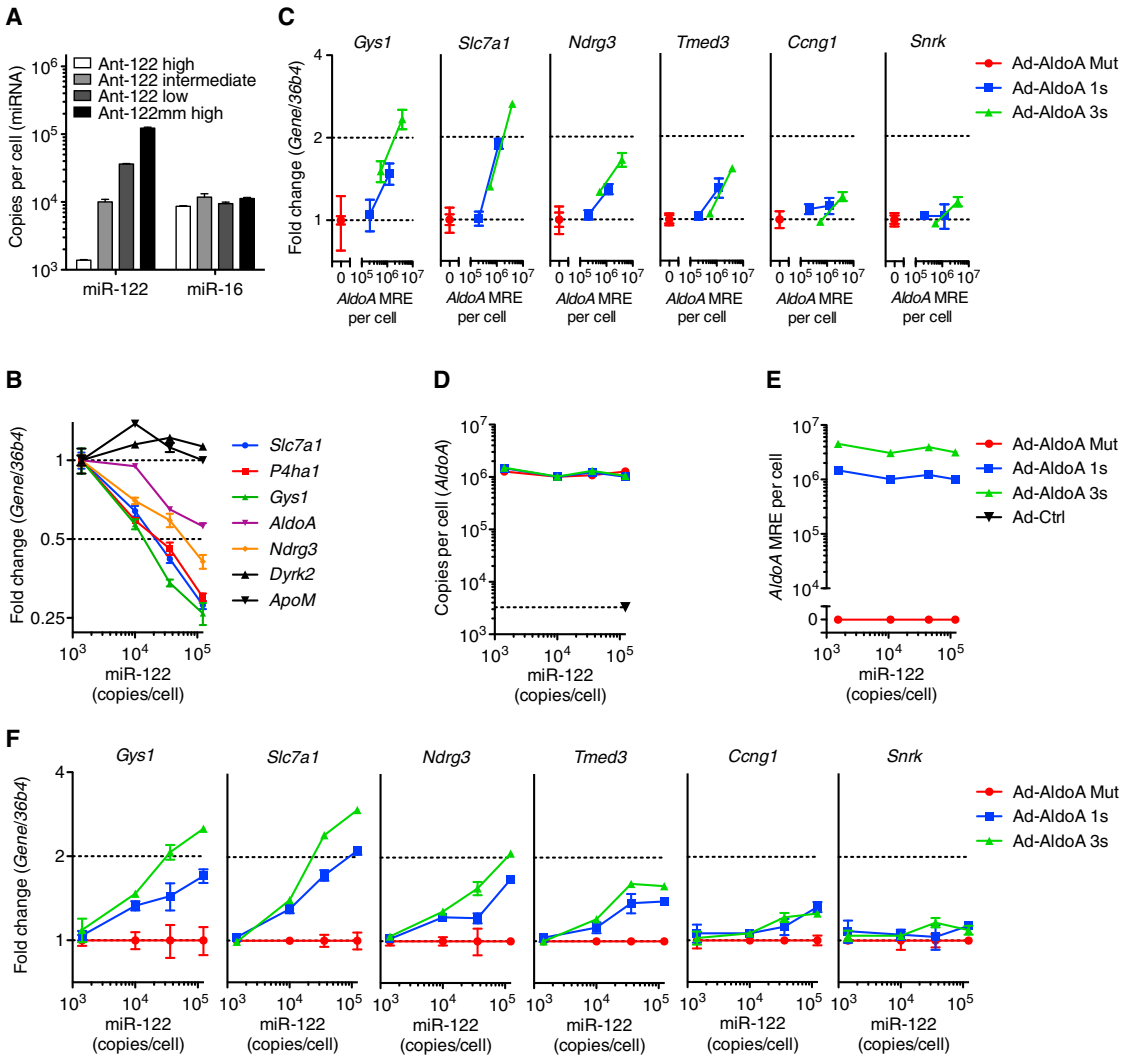

Figure 2. The High Threshold Persists after Lowering miR-122 Activity

(A) Absolute miRNA copy numbers per cell or (B) relative expression of miR-122 target genes and control nontarget genes (*Dyrk2* and *ApoM*) in primary hepatocytes from mice treated with Ant-122mm or different concentrations of Ant-122. Values for miR-122 target and control genes are normalized to that of the lowest miR-122 concentration.

(C) Relative expression of miR-122 target genes and a nontarget gene (*Snrk*) in primary hepatocytes with 3-fold decreased miR-122 levels shown in (A), infected with MOI 20 and 200 of Ad-AldoA Mut (red), 1s (blue), or 3s (green).

(D–F) Primary hepatocytes shown in (A) infected with MOI 200 of the three Ad-AldoA constructs. Absolute copy numbers per cell of *AldoA* (D) and *AldoA* MRE (E) in relation to miR-122 copy numbers.

(F) Relative expression of miR-122 target genes and control nontarget gene (*Snrk*) normalized to Ad-AldoA Mut of the respective miR-122 condition.

Absolute miRNA copy numbers were calculated by multiplying relative abundance (miRNA/snoRNA202) that were normalized to Ant-122mm with the copy number evaluated in Figure 1B. Data represent mean ± SEM (n = 4) for all panels.

not the number of miRNA molecules. Thus, in this scenario, miRNA reduction would lower the degree to which targets are repressed, but it would not lower the threshold of added MREs required to observe derepression.

By analyzing whether a change in miRNA levels influences the threshold for the number of added *AldoA* MREs needed for derepression, we sought to experimentally evaluate which scenario applies. We injected three different amounts (low, intermediate, and high) of Antagomir-122 (Ant-122) into mice and found that miR-122 levels detected in the primary hepatocytes were reduced to 0.3, 0.08, and 0.01 of that observed in hepatocytes from mice injected with the mismatch Ant-122 control (Ant-122mm; Figure 2A) (Krützfeldt et al., 2005). Target gene derepression correlated with decreased miR-122 levels, which confirmed that our miR-122 quantification reflected miR-122 activity (Figure 2B). Next, we studied the effect of controlled overexpression of *AldoA* MRE on target gene derepression in hepatocytes with a modest 3-fold decrease in miR-122 levels. Interestingly, derepression was detected only when exceeding the threshold of 2 × 10^5 *AldoA* MREs per cell (Figure 2C). This

threshold was comparable to that observed in cells without reduced miR-122 levels, which indicated that the reason for the threshold was not excess miR-122 binding capacity. Instead, high TA is the more likely reason that the amount of added MREs must exceed a very high level before exerting an observable effect.

Some studies claiming ceRNA-mediated gene regulation focus on the number of sites to miRNA families that are shared between the ceRNAs without differentiating between those miRNAs that are expressed at a level sufficient to repress target genes and those that are not (Jeyapalan et al., 2011; Fang et al., 2013). To demonstrate that derepression can only occur in conditions in which target gene repression is happening, we infected hepatocytes harboring different miR-122 levels with Ad-AldoA at MOI 200 and measured target derepression. Levels of *AldoA* and respective *AldoA* MRE copy number per cell were comparable in all Ant-treated samples (Figures 2D and 2E). miR-122 target gene derepression was between 1.5- and 2.5-fold in hepatocytes with high miR-122 levels and below 1.5-fold in cells with intermediate miR-122 activity (Figure 2F). No target gene derepression was observed in hepatocytes with the lowest miR-122 levels. Altogether, these data demonstrate that miRNAs need to exceed an expression level sufficient to repress their targets in order for targets to be derepressed in a ceRNA-dependent manner.

The Magnitude of Derepression Correlates with Predicted Site Efficacy and Number of Added *AldoA* MREs

Previous ceRNA studies have focused on only one or a few targets of a miRNA even though a ceRNA change that influences miRNA activity would be expected to affect more than a few targets. Because any perturbation of a cell might result in spurious expression changes in a few predicted targets, a transcriptome-wide analysis examining the preferential effect on predicted targets would more confidently detect the influence of a competing RNA. Therefore, we extended our quantitative analysis to the transcriptome and performed RNA sequencing (RNA-seq) on primary hepatocytes infected with different Ad-AldoA constructs at MOI 2, 20, and 200. Then, we analyzed the relationship between the derepression of predicted targets and their site number, site type (6, 7, and 8 nt sites), site position, and other determinants used by TargetScan to calculate total context+ scores of predicted miRNA targets (Lewis et al., 2005; Grimson et al., 2007; Garcia et al., 2011). When predicted targets of miR-122, miR-33, miR-16, or abundant miRNA families in liver (either let-7, miR-192, or a combination of the next four most abundant families) were distributed into ten context+ score bins and plotted against their median fold change, the effect of target derepression was evident for predicted targets of miR-122 but not for those of any of the other miRNA families (Figures 3A, S3A, S3B, and Table S1). As expected, the extent of target derepression correlated with the magnitude of the context+ score as well as with the number of added *AldoA* MREs. These correlations were also observed in the fold change distributions of miR-122 predicted targets (Figure 3B), and analogous results were obtained when stratifying predicted targets by site type (Figure S3C). Regardless of how we grouped the predicted targets, the same threshold of $\geq 1.5 \times 10^5$ added MREs per cell was required in order to observe miR-122 derepression. We also studied target gene derepression in primary hepatocytes treated with Ant-122 or the mismatch control Ant-122mm and found that the strongest predicted targets (e.g., those with a context+ scores below –0.2) were significantly derepressed in the Ant-122-treated conditions (Figures S3D–S3G and Table S1).

Modest Changes in Target Abundance Are Induced by Metabolic Stress and Disease

Next, we sought to investigate the quantitative relationship between MREs added upon Ad-AldoA infection and those normally contributed by mRNAs of primary hepatocytes. First, we tested how transcript abundances, measured by RNA-seq in fragments per kilobase of transcript per million fragments mapped (FPKM) correlated with the absolute copy numbers determined by quantitative PCR. To this end, we compared the expression levels of four genes that are differentially expressed in primary hepatocyte and liver samples and found a linear relationship between FPKM and absolute copy numbers over several orders of magnitude (Figure 4A), which allowed us to transform RNA-seq data to absolute mRNA copies per cell. Then, we compared how *AldoA* transcript abundance corresponded to genome mRNA abundance at different MOIs of Ad-AldoA-infected hepatocytes. The *AldoA* contribution ranged from 0.3%–0.8% at MOI of 2, 6%–12% at MOI 20, and > 50% of all mRNA at MOI 200 (Figure 4B). In contrast, the largest endogenous contributor to the transcriptome of primary hepatocytes was Transferrin (*Trf*), which made up only 1.6% of the mRNA (30,000 molecules per cell). Thus, the level of *AldoA* at the MOI for which derepression was observed (MOI 20 and 200), was substantially higher than that of transcripts from any single cellular gene.

We also attempted to place the *AldoA* abundance within the context of the miR-122 TA within the hepatocyte transcriptome. A previous estimate of miRNA TA considers all of the 7 and 8 nt sites for that miRNA within expressed 3′ UTRs (Garcia et al., 2011). This TA might over- or underestimate the effective number of binding sites of the transcriptome, depending on the extent to which some of these sites are inaccessible (e.g., because they are occluded by mRNA secondary structure or RNA binding proteins) and the extent to which intracellular binding capacity is augmented by additional sites (e.g., 6 nt sites, other marginal sites, and nonconventional sites as well as sites in ORFs, 5′ UTRs, or noncoding RNAs), many of which might add to the effective number of binding sites without mediating repression. Despite these uncertainties, relative TA estimates for different miRNAs provide a useful basis for distinguishing the more effective miRNAs from the less effective ones (Garcia et al., 2011).

Our conclusion that competing MREs begin to exert their effects as they approach the miRNA binding capacity of the transcriptome provided the means to evaluate the relationship between the previous TA estimate and the apparent number of binding sites. When calculated as before (summing 7 and 8 nt sites in transcriptome 3′ UTRs), the miR-122 TA in hepatocytes at Ad-AldoA MOI 2 was 1.8×10^5 sites per cell, which essentially matched the threshold of added MREs required to begin to observe derepression. The addition of 6 nt sites in the analysis increased the number to 4.4×10^5 miR-122 sites per cell. Given that this was still below the number of added MREs required to

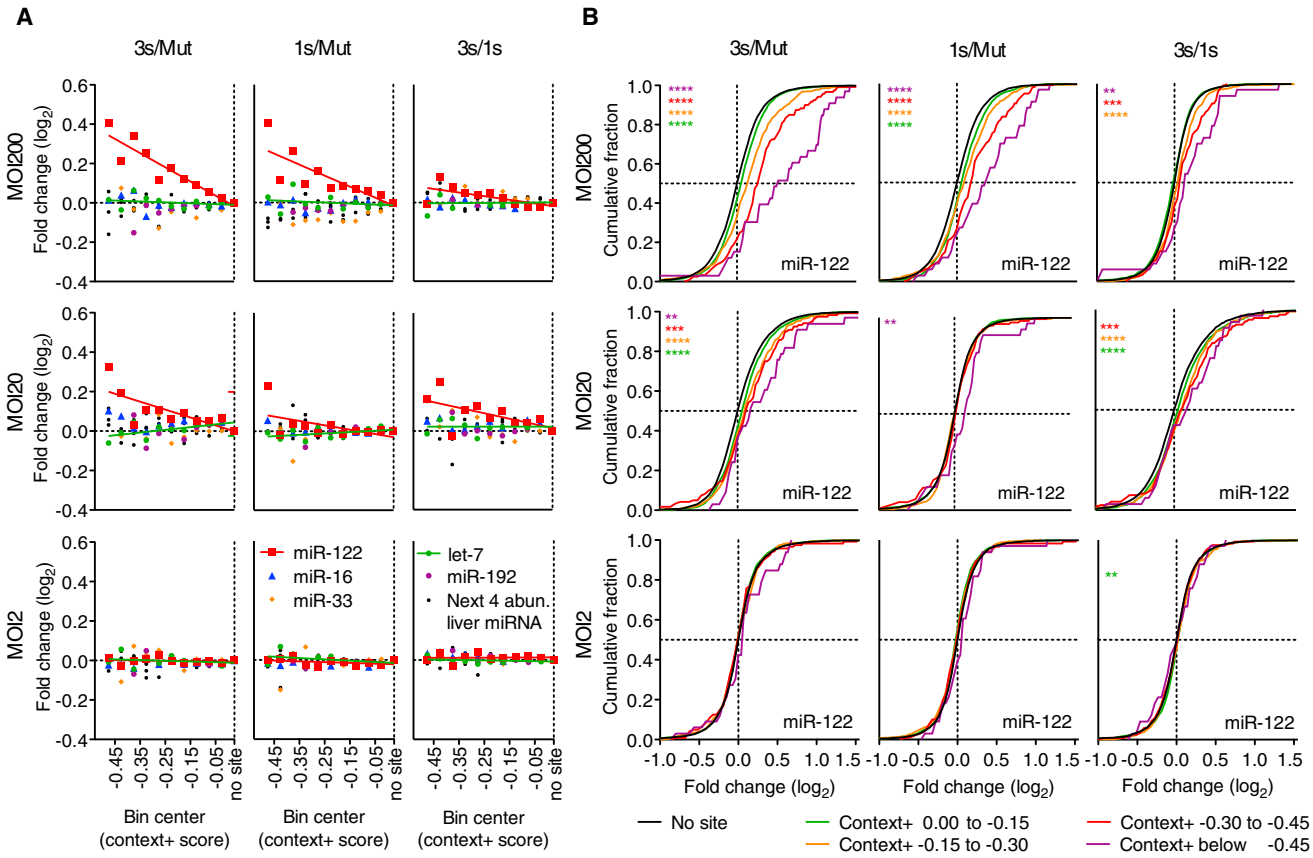

Figure 3. The Magnitude of Derepression Correlates with Predicted Site Efficacy and Number of Added *AldoA* MREs

(A and B) RNA-seq results showing derepression of predicted targets from primary hepatocytes infected with MOI 200, 20, and 2 of Ad-AldoA Mut, 1s, or 3s shown in Figures 1C–1H.

(A) Predicted targets of miR-122 (red), miR-16 (blue), miR-33 (orange), let-7 (green), miR-192 (purple), or a combination of the next four most abundant liver miRNA families (black) were grouped into ten bins based on their context+ scores. For each miRNA family, the median $\log_2$ fold change is plotted for the predicted targets in each bin. Medians were normalized to that of the bin with genes without sites. Bins each had at least ten genes; see Figure S3B for group sizes.

(B) Cumulative distributions of mRNA changes for genes with no miR-122 site (black) or predicted target genes with the indicated context+ score bins (color). Number of genes per bin: black, 6,629; green, 1,693; orange, 434; red, 120; purple, 33. *p < 0.05, **p < 0.01, ***p < 0.001, ****p < 0.0001, one-sided Kolmogorov-Smirnov (K-S) test.

See also Figure S3 and Table S1.

observe half-maximal derepression, for all additional analyses, we considered this revised TA estimate (all 6, 7, and 8 nt sites within the transcriptome 3′ UTRs), which we define as the apparent TA (or TA_{app}), as a conservative estimate of the effective number of miRNA sites.

Next, we calculated how *AldoA* MREs influenced the miR-122 TA_{app} (Figure 4C) and what fraction of the TA_{app} *AldoA* MREs contributed (Figure 4D). Because only very highly expressed genes could reach the levels required to affect TA, we searched for endogenous transcripts that quantitatively contributed the largest percentage to transcriptome TA_{app}. *Actinb* (*Actb*), which contributed 5.5% of the TA_{app}, was the largest potential contributor to miR-122 site abundance in primary hepatocytes (Figure 4E), although this contribution was less than the 30% contribution required for *AldoA* to detectably modulate miR-122 repression (Figure 4D). When using the same approach to estimate TA_{app} for let-7, miR-16, miR-33, miR-192, or each of the next four most abundant miRNA families, the transcript with the largest contribution to any TA_{app} was Albumin (*Alb*), which contributed ~3% of the miR-103 TA_{app} (Figure 4E).

As a major metabolic integrator of physiological processes, the liver exhibits profound changes of gene regulation in response to insulin signaling and cholesterol metabolism. To examine whether these changes might affect miRNA TA_{app}, we analyzed two models with severe pathological changes in cholesterol metabolism (LDLR-deficient mice, *Ldlr*$^{-/-}$) (Ishibashi et al., 1993) and hepatic steatosis (high-fat diet [HFD] mice; Figures 4F, S4A, and Table S2) (Channon and Wilkinson, 1936). We also examined livers that were perfused in the absence and presence of insulin, representing fasted and fed states, respectively (Figure S4B and Table S2). In all livers studied, *Alb* and Transthyretin (*Ttr*) contributed ~10%–20% to TA_{app}. The only strong contributor that was differentially regulated in any model was major urinary protein 7 (*Mup7*), which essentially disappeared

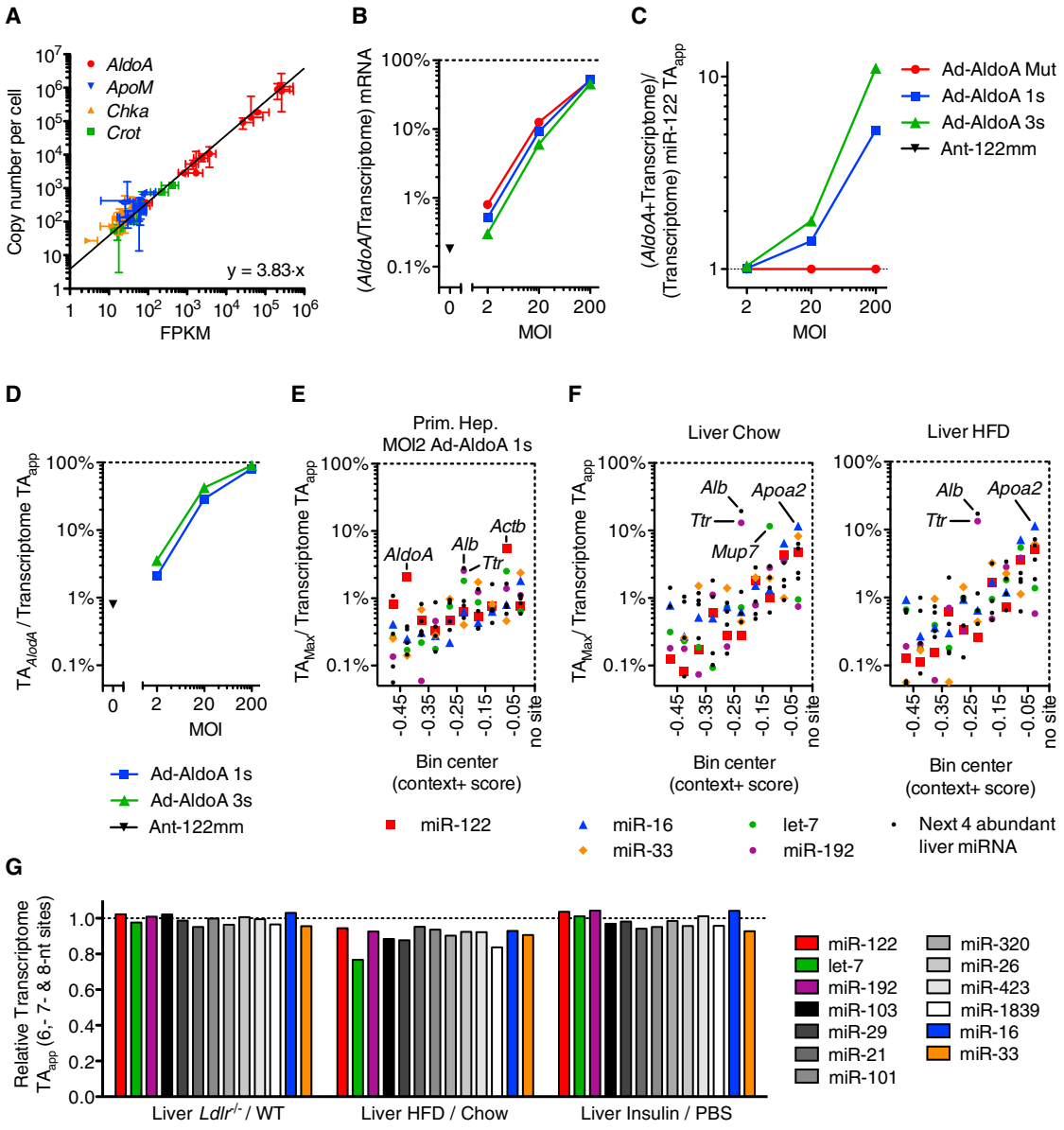

Figure 4. Modest Changes in Target Abundance Are Induced by Metabolic Stress and Disease

(A) Relationship between FPKM from RNA-seq data and absolute quantification with qPCR. Represented are four genes quantified in all 11 primary hepatocyte samples plus wild-type and *Ldlr*$^{-/-}$ liver samples. Line represents linear regression of data points. Data represent mean ± 95% confidence intervals.

(B–D) RNA-seq data from primary hepatocytes infected with MOI 200, 20, and 2 of Ad-AldoA Mut, 1s, or 3s shown in Figure 1C–H. Data represent mean ± SEM (B). Contribution of *AldoA* mRNA to the sum of genome mRNA. Increase of transcriptome miR-122 TA_{app} (C) and the respective contribution of *AldoA* MRE (D) to total transcriptome miR-122 TA_{app} mediated by the different Ad-AldoA constructs and viral concentrations.

(E and F) Fractional contribution of the largest potential contributors to transcriptome TA_{app} in primary hepatocytes infected with MOI 2 of Ad-AldoA 1s (E) or in wild-type livers (F) originated from mice either fed normal chow or high-fat diet (HFD). Potential contributors were binned by their context+ scores, and the top potential contributors are plotted within each bin. See also Figure S4 and Table S2.

(G) Relative target abundance of livers from models of physiological (insulin) or disease/stress states (*Ldlr*$^{-/-}$ and HFD).

in livers of HFD mice, causing its contribution to TA_{app} to decrease from 11.6% in normal livers to 0.01% in HFD livers. *Alb*, the most highly expressed mRNA and the largest potential contributor of sites for the miR-103 family, had the potential to reduce TA_{app} by a maximum of only 20% when fully silenced. Conversely, a 30% increase in target abundance would require the most abundant liver transcript to increase ~2.5-fold.

Because none of the small number of genes that alone could alter TA_{app} in a consequential way appeared to do so, we tested whether a substantial change could be achieved through collective changes of all mRNAs. Evaluation of TA_{app} changes for

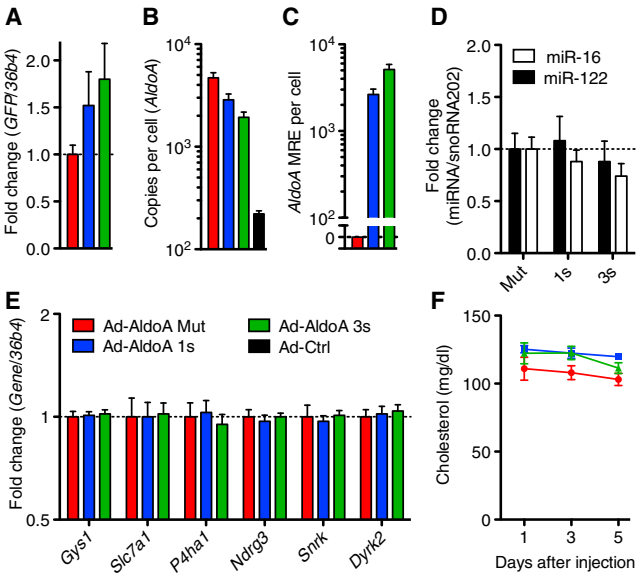

Figure 5. No ceRNA Effect Is Detected In Vivo

(A–E) Mice were injected with Ad-AldoA Mut (red, n = 6), 1s (blue, n = 6), or 3s (green, n = 5), and gene expression analysis was performed 5 days post-infection. Relative gene expression of *GFP* (A), absolute copy numbers per cell of *AldoA* (B), and added *AldoA* MREs (C). Relative expression of miRNAs (D) and miR-122 target genes or control nontarget genes (*Snrk* and *Dyrk2)* (E). (F) Plasma cholesterol levels of Ad-AldoA-treated mice at days 1, 3, and 5. The Ad-AldoA used in this experiment expressed the full-length protein. Data represent mean ± SEM.

miR-122, the next ten most abundant miRNA families in liver, miR-33, and miR-16 revealed that TA_{app} values for these miRNAs were not altered more than 25% in any physiological or disease model, and most changes were below 10% (Figure 4G). We also calculated TA_{app} values for the liver samples and primary hepatocytes infected with Ad-AldoA at MOI 20, in which derepression was observed. Transcriptome TA_{app} values ranged between 2.5–7.5 × 10^5 sites per cell in liver models, and between 3.6–13 × 10^5 in primary hepatocytes (Figure S4C).

No ceRNA Effect Is Detected In Vivo

To examine the influence of *AldoA* MREs on target gene derepression and relevant physiological endpoints in vivo, we injected wild-type mice with 3 × 10^9 plaque-forming units of Ad-AldoA and examined livers 5 days postinfection. Virally expressed *GFP*, and therefore adenovirus expression, was comparable in all conditions (Figure 5A). Ad-AldoA increased *AldoA* transcripts from 2.2 × 10^2 (endogenous levels) to 4.7 × 10^3 copies per cell (Figure 5B), introducing between 2.6 × 10^3 and 5.1 × 10^3 miR-122 MREs per cell with Ad-AldoA 1s or 3s, respectively (Figure 5C). Overexpression of the Ad-AldoA constructs did not change levels of miR-122 or a control miRNA (Figure 5D). No derepression of any miR-122 target or control gene (*Snrk* and *Dyrk2*) was observed (Figure 5E). Furthermore, we did not detect changes in serum cholesterol levels (Figure 5F), which decrease upon miR-122 inhibition by Ant-122 (Krützfeldt et al., 2005). As predicted from our studies of primary hepatocytes, these results showed that introduction of 5.1 × 10^3 miR-122 MREs per cell was insufficient to induce either target derepression or downstream physiological responses.

DISCUSSION

Our results support a model in which the changes in ceRNAs must begin to approach the TA of miRNA before they can exert a consequential effect on the repression of targets for that miRNA. For miR-122 in hepatocytes, derepression began to be observed at a threshold of 1.5 × 10^5 added sites per cell, a value exceeding the physiological levels of any endogenous target as well as the aggregate change of all predicted targets in different disease states. Altogether, our data imply that a ceRNA effect mediated through a single miRNA family in a physiological or disease setting of the liver is unlikely. However, we cannot exclude the possibility that unidentified highly abundant and regulated noncoding RNAs (including circRNAs) might substantially contribute to the pool of transcriptome binding sites.

In stating that changes in endogenous targets are unlikely to mediate a ceRNA effect that is detectable, we do not mean to imply that there is absolutely no molecular consequence of changing the level of an endogenous target. Large changes in each of several dozen target genes could alter TA by 1% or sometimes more, which would influence the repression of other targets but not to an extent that would be detectable by our methods. For example, an increase in TA by 5% is expected to decrease repression of other targets by approximately 5%, causing a target that was previously repress by 30% to now be repressed by approximately 28.5%—a change too small to be detected and presumably too small to be of biological consequence.

Studying the stoichiometric relationship of an miRNA and its TA and assessing the effect of this relationship on target gene regulation has been challenging. Estimates of TA have proven to be particularly difficult, given that the extent to which ineffective or marginally effective binding sites contribute to TA has been unclear, and no experimentally determined TA values had been obtained. Our experiments indicate that the TA_{app} for miR-122 in the hepatocyte transcriptome is 4.4 × 10^5 sites per cell. Although this estimate corresponds to the number of ≥6 nt seed-matched sites for miR-122 in the 3′ UTRs, we do not presume that all UTR sites mediate repression. Indeed, the TA_{app} is expected to exceed the number of miR-122 MREs, given that sites that bind the miRNA too transiently to exert repression (including most sites in ORFs) would nonetheless contribute to TA_{app}.

We qualify our TA estimate as an "apparent TA" for two reasons: first, our miR-122 TA_{app} is expected to be a function of the strength of the miR-122 site that was used in its determination. The *AldoA* site is relatively strong (context+ score of −0.4; Figure 4E). Had we empirically estimated the TA with a weaker miR-122 site, more of the added sites would have been required to approach half derepression, and thus the TA_{app} value would have been correspondingly higher. Second, the endogenous sites contribute to TA_{app} in proportion to their ability to sequester the miRNA, and thus because many weak sites (ranging from those typically classified as nonspecific sites to those that might be more specific yet nonetheless ineffective or marginally

effective) each make partial contributions to the TA_{app}, the actual number of sites that contributed is expected to greatly exceed the TA_{app}. When considering this second point, estimating a TA_{app} is of greater practical value than knowing the total number of endogenous sites that helped sequester the miRNA.

Our miR-122 TA_{app} was empirically derived on the premise that using Ad-AldoA to double the effective miR-122 TA and thereby decrease the number of encounters between miR-122 and its endogenous targets by half would lead to a corresponding decrease in endogenous target repression. If the amount of miR-122-mediated repression is not a simple linear function of the number of encounters with its targets, then TA_{app} would need to be corrected accordingly. For other miRNAs, TA_{app} values were estimated starting with the miR-122 TA_{app} and assuming that relative values for different miRNAs would scale in proportion to their numbers of UTR sites—an assumption supported by studies showing that miRNA efficacy negatively correlates with the relative numbers of UTR sites (Arvey et al., 2010; Garcia et al., 2011; Mullokandov et al., 2012). Despite any uncertainty arising from these simplifying assumptions, our TA_{app} estimates have the unique benefit of being founded on intracellular experimental observations.

This experimental grounding produced TA_{app} values much higher than those previously assumed. For example, previous modeling of the quantitative relationships between miRNAs and their targets assumed that a typical miRNA had ~500 target sites per cell (Wee et al., 2012). Modeling based on this low number of targets suggests that for moderately expressed miRNAs, adding only 500 sites through increased ceRNA expression could double the expression of a repressed mRNA, whereas for more highly expressed miRNAs, many more sites would be required to exert an effect (Mullokandov et al., 2012; Wee et al., 2012). Our results in hepatocytes indicate that TA_{app} values for the eleven most abundant miRNA families ranged from 2.5×10^5 to 7.5×10^5 sites, about 1,000 times greater than the value previously assumed. This substantially revised estimate of effective TA leads to a different and somewhat simplified picture of the potential for regulation through ceRNAs. In our model, miRNA levels matter only in so much as the miRNA must reach a level sufficient to repress a target mRNA. For any miRNA exceeding this level, the potential for ceRNAs to influence repression is simply a matter of whether the ceRNAs add or subtract enough sites to meaningfully influence the TA_{app}. Because TA_{app} is a function of the number of seed-matched sites in the transcriptome and substantially exceeds the level of even the most highly expressed miRNA, the ceRNA difference required to achieve half-maximal effects is independent of the miRNA level. Thus, our insights and results indicate that repression by even moderately expressed miRNAs would be difficult to detectably change through a ceRNA effect.

Under extreme physiological and disease conditions, target abundances were not changed more than 10% for most miRNA families. The maximum change of ~25% was observed for the let-7 miRNA family in mice fed an HFD versus a chow diet. Interestingly, in this condition, a single highly expressed gene (*Mup7*) accounted for ~50% of the total decrease in let-7 target abundance. A recent phase I trial for RNAi therapy of Ttr amyloidosis reduced human TTR levels by >80% (Coelho et al., 2013). Such a strong reduction of the *TTR* transcript, which contributes ~10% of the miR-192 TA_{app} in mouse livers, would account for a decrease in miR-192 target abundance analogous to that observed for *Mup7* and let-7 in the HFD versus chow diet, a change not expected to detectably affect miRNA activity.

The conclusion that only large contributors to TA_{app} can detectably influence the miRNA activity agrees with our in vivo experiments; in normal liver, *AldoA* is expressed at $\sim 2.4 \times 10^2$ copies per cell and is among the thousand most highly expressed genes. Still, a 9-fold increase in transcript levels after Ad-AldoA 3s infection, which added $\sim 5 \times 10^3$ MREs, increased miR-122 TA_{app} by only 2% and therefore imparted no detectable influence on target gene expression. *Mup7* and *Ttr* are among the thirty genes expressed in liver at copy numbers above 10^4 copies per cell, and therefore approaching within an order of magnitude the estimated miRNA TA_{app} values. Hence, only these 30 genes have potential on their own to perceptibly influence a TA_{app}.

Our study focused on miR-122, an unusually highly expressed miRNA. Nonetheless, the same high threshold for detectable target derepression was observed when miR-122 activity was reduced, which indicated that our conclusions apply also to more moderately expressed miRNAs. A study reporting loss of miR-20 repression when adding high levels of target mRNA also observed a threshold at high target expression (Mukherji et al., 2011). As expected, their threshold disappeared when a miR-20 sponge was used to lower miRNA activity below detection. More interestingly, they found that transfecting an miR-20 mimic increased the threshold for derepression. A possible reason that they observed a change in threshold with a change in miRNA, whereas we did not, is that their miR-20 mimic might have added enough miRNA to exceed the miR-20 TA_{app} of their cells. Another difference between their experiments and ours is that their target contained bulged sites of a type that can induce miRNA degradation (Ameres et al., 2010), which might produce an apparent shift in the threshold.

Gene expression in the liver is profoundly regulated by circadian and hormonal and nutritional states. Using livers of mice exposed to insulin signaling and to pathological conditions of cholesterol metabolism, we did not observe large changes in target abundance, raising the possibility that our findings can be generalized to other organs and disease states. Nonetheless, during cell differentiation and in the context of malignant transformation, expression of coding and noncoding RNA can change dramatically (Rhodes and Chinnaiyan, 2005; Lujambio and Lowe, 2012). In such biological settings conditions might arise in which TA_{app} is lower than in physiological settings and/or a single mRNA substantially contributes to target abundance. In principle, such alterations could make the system more amenable to ceRNA-mediated gene regulation.

EXPERIMENTAL PROCEDURES

Animal Experiments

Animals were maintained on a 12 hr light/12 hr dark cycle under a controlled environment in a pathogen-free facility at the Institute for Molecular Systems Biology, ETH Zürich. Mice were administered adenovirus through a single

tail-vein injection of 3 × 10^9 plaque-forming units in a final volume of 0.2 ml diluted in PBS and killed 5 days postinjection. Antagomir was administered through tail-vein injections on three consecutive days, and primary hepatocytes were isolated on day four. For high, intermediate, and low miR-122 inhibition, mice received 3 × 80, 40, and 20 mg/kg Ant-122, respectively. Ant-122mm (control) was used at the highest concentration. All animal experiments were approved by the ethics committee of the Kantonale Veterinäramt Zürich.

Primary Hepatocytes Isolation and Viral Infections

Primary hepatocytes of 8- to 12-week-old male C57BL/6N mice were isolated on the basis of the method described by Zhang et al. (2012). Hepatocytes were counted and plated at 300,000 cells per well in Dulbecco's modified Eagle's medium low-glucose media and adenoviruses were added in Hepatozyme media 4–6 hr after plating and harvested 24 hr postinfection. All cells were incubated at 37°C in a humidified atmosphere containing 5% CO_2.

Adenoviruses

Recombinant adenoviruses were generated as described in the Supplemental Experimental Procedures. All adenoviruses expressed *GFP* from an independent promoter. Ad-Ctrl was based on the same vector backbone (including GFP) but lacked the *AldoA* transgene.

Gene Expression Analysis

2 ug of total RNA was treated with the DNA-*free* Kit (Life Technologies) and reverse transcribed with the High Capacity cDNA Reverse Transcription Kit (Life Technologies). Quantitative PCR reactions were performed with the LightCycler 480 (Roche) employing KAPA SYBR FAST qPCR Master Mix (2×) for LightCycler 480 (Kapa Biosystems) and gene-specific primer pairs (Table S3). Relative gene expression was calculated with the ddCT method and mouse *36b4* (*Rplp0*) for normalization.

miRNA Expression Analysis

150 ng of total RNA was reverse-transcribed with the TaqMan MicroRNA Assays and Reverse Transcription Kits (Life Technologies). Quantitative PCR reactions were performed with the LightCycler 480 employing TaqMan Universal PCR Master Mix, No AmpErase UNG (Life Technologies), and TaqMan MicroRNA Assays (Life Technologies). Relative miRNA expression was calculated with the ddCT method and mouse snoRNA202 for normalization.

RNA-Seq

For single-end library construction, total RNA was depleted of rRNA with the Ribo-Zero rRNA Removal Kit (Epicenter). RNA libraries were prepared with the dUTP-based, Illumina-compatible NEXTflex Directional RNA-Seq Kit (Bioo Scientific). For paired-end library construction (performed by BGI), total RNA was enriched for poly(A) mRNA with oligo(dT) beads and treated with buffer in order to yield 200–700 nt fragments. First-strand cDNA was synthesized with random hexamer primers, and second-strand cDNA was synthesized with buffer, dNTPs, RNase H, and DNA polymerase I. cDNA was run on an Agarose gel for suitable fragment size selection followed by a purification, adaptor ligation, and PCR amplification. All libraries (both single- and paired-end) were sequenced with an Illumina HiSeq 2000 sequencing machine.

ACCESSION NUMBERS

The NCBI Gene Expression Omnibus accession number for the data reported in this paper is GSE52801.

SUPPLEMENTAL INFORMATION

Supplemental Information contains Supplemental Experimental Procedures, four figures, and three tables and can be found with this article online at http://dx.doi.org/10.1016/j.molcel.2014.03.045.

ACKNOWLEDGMENTS

We would like to thank M. Ravichandran and W. Johnston for technical assistance as well as D. Koppstein, V. Auyeung, M. Latreille, and members of the D.P.B. and M.S. labs for critically reviewing this manuscript. This material is based upon work supported under a National Science Foundation Graduate Research Fellowship (to V.A.), an ERC grant (Metabolomirs) and the NCCR (RNA and Biology; to M.S.), and NIH grant GM067031 (to D.P.B.). D.P.B. is a Howard Hughes Medical Institute Investigator. D.P.B. and M.S. are members of the scientific advisory boards of Alnylam Pharmaceuticals and Regulus Therapeutics.

Received: January 7, 2014
Revised: March 4, 2014
Accepted: March 19, 2014
Published: May 1, 2014

REFERENCES

Ala, U., Karreth, F.A., Bosia, C., Pagnani, A., Taulli, R., Léopold, V., Tay, Y., Provero, P., Zecchina, R., and Pandolfi, P.P. (2013). Integrated transcriptional and competitive endogenous RNA networks are cross-regulated in permissive molecular environments. Proc. Natl. Acad. Sci. USA *110*, 7154–7159.

Ameres, S.L., Horwich, M.D., Hung, J.H., Xu, J., Ghildiyal, M., Weng, Z., and Zamore, P.D. (2010). Target RNA-directed trimming and tailing of small silencing RNAs. Science *328*, 1534–1539.

Arvey, A., Larsson, E., Sander, C., Leslie, C.S., and Marks, D.S. (2010). Target mRNA abundance dilutes microRNA and siRNA activity. Mol. Syst. Biol. *6*, 363.

Baek, D., Villén, J., Shin, C., Camargo, F.D., Gygi, S.P., and Bartel, D.P. (2008). The impact of microRNAs on protein output. Nature *455*, 64–71.

Bissels, U., Wild, S., Tomiuk, S., Holste, A., Hafner, M., Tuschl, T., and Bosio, A. (2009). Absolute quantification of microRNAs by using a universal reference. RNA *15*, 2375–2384.

Brenner, J.L., Jasiewicz, K.L., Fahley, A.F., Kemp, B.J., and Abbott, A.L. (2010). Loss of individual microRNAs causes mutant phenotypes in sensitized genetic backgrounds in *C. elegans*. Curr. Biol. *20*, 1321–1325.

Cesana, M., Cacchiarelli, D., Legnini, I., Santini, T., Sthandier, O., Chinappi, M., Tramontano, A., and Bozzoni, I. (2011). A long noncoding RNA controls muscle differentiation by functioning as a competing endogenous RNA. Cell *147*, 358–369.

Channon, H.J., and Wilkinson, H. (1936). The effect of various fats in the production of dietary fatty livers. Biochem. J. *30*, 1033–1039.

Coelho, T., Adams, D., Silva, A., Lozeron, P., Hawkins, P.N., Mant, T., Perez, J., Chiesa, J., Warrington, S., Tranter, E., et al. (2013). Safety and efficacy of RNAi therapy for transthyretin amyloidosis. N. Engl. J. Med. *369*, 819–829.

Ebert, M.S., Neilson, J.R., and Sharp, P.A. (2007). MicroRNA sponges: competitive inhibitors of small RNAs in mammalian cells. Nat. Methods *4*, 721–726.

Esau, C., Davis, S., Murray, S.F., Yu, X.X., Pandey, S.K., Pear, M., Watts, L., Booten, S.L., Graham, M., McKay, R., et al. (2006). miR-122 regulation of lipid metabolism revealed by in vivo antisense targeting. Cell Metab. *3*, 87–98.

Eulalio, A., Huntzinger, E., and Izaurralde, E. (2008). Getting to the root of miRNA-mediated gene silencing. Cell *132*, 9–14.

Fang, L., Du, W.W., Yang, X., Chen, K., Ghanekar, A., Levy, G., Yang, W., Yee, A.J., Lu, W.Y., Xuan, J.W., et al. (2013). Versican 3′-untranslated region (3′-UTR) functions as a ceRNA in inducing the development of hepatocellular carcinoma by regulating miRNA activity. FASEB J. *27*, 907–919.

Farh, K.K., Grimson, A., Jan, C., Lewis, B.P., Johnston, W.K., Lim, L.P., Burge, C.B., and Bartel, D.P. (2005). The widespread impact of mammalian MicroRNAs on mRNA repression and evolution. Science *310*, 1817–1821.

Figliuzzi, M., Marinari, E., and De Martino, A. (2013). MicroRNAs as a selective channel of communication between competing RNAs: a steady-state theory. Biophys. J. *104*, 1203–1213.

Franco-Zorrilla, J.M., Valli, A., Todesco, M., Mateos, I., Puga, M.I., Rubio-Somoza, I., Leyva, A., Weigel, D., García, J.A., and Paz-Ares, J. (2007). Target mimicry provides a new mechanism for regulation of microRNA activity. Nat. Genet. *39*, 1033–1037.

Friedman, R.C., Farh, K.K.H., Burge, C.B., and Bartel, D.P. (2009). Most mammalian mRNAs are conserved targets of microRNAs. Genome Res. *19*, 92–105.

Garcia, D.M., Baek, D., Shin, C., Bell, G.W., Grimson, A., and Bartel, D.P. (2011). Weak seed-pairing stability and high target-site abundance decrease the proficiency of lsy-6 and other microRNAs. Nat. Struct. Mol. Biol. *18*, 1139–1146.

Giraldez, A.J., Mishima, Y., Rihel, J., Grocock, R.J., Van Dongen, S., Inoue, K., Enright, A.J., and Schier, A.F. (2006). Zebrafish MiR-430 promotes deadenylation and clearance of maternal mRNAs. Science *312*, 75–79.

Grimson, A., Farh, K.K., Johnston, W.K., Garrett-Engele, P., Lim, L.P., and Bartel, D.P. (2007). MicroRNA targeting specificity in mammals: determinants beyond seed pairing. Mol. Cell *27*, 91–105.

Guo, H., Ingolia, N.T., Weissman, J.S., and Bartel, D.P. (2010). Mammalian microRNAs predominantly act to decrease target mRNA levels. Nature *466*, 835–840.

Hafner, M., Landthaler, M., Burger, L., Khorshid, M., Hausser, J., Berninger, P., Rothballer, A., Ascano, M., Jr., Jungkamp, A.C., Munschauer, M., et al. (2010). Transcriptome-wide identification of RNA-binding protein and microRNA target sites by PAR-CLIP. Cell *141*, 129–141.

Hansen, T.B., Jensen, T.I., Clausen, B.H., Bramsen, J.B., Finsen, B., Damgaard, C.K., and Kjems, J. (2013). Natural RNA circles function as efficient microRNA sponges. Nature *495*, 384–388.

Ishibashi, S., Brown, M.S., Goldstein, J.L., Gerard, R.D., Hammer, R.E., and Herz, J. (1993). Hypercholesterolemia in low density lipoprotein receptor knockout mice and its reversal by adenovirus-mediated gene delivery. J. Clin. Invest. *92*, 883–893.

Jeyapalan, Z., Deng, Z., Shatseva, T., Fang, L., He, C., and Yang, B.B. (2011). Expression of CD44 3′-untranslated region regulates endogenous microRNA functions in tumorigenesis and angiogenesis. Nucleic Acids Res. *39*, 3026–3041.

Jopling, C.L., Yi, M., Lancaster, A.M., Lemon, S.M., and Sarnow, P. (2005). Modulation of hepatitis C virus RNA abundance by a liver-specific MicroRNA. Science *309*, 1577–1581.

Karreth, F.A., Tay, Y., Perna, D., Ala, U., Tan, S.M., Rust, A.G., DeNicola, G., Webster, K.A., Weiss, D., Perez-Mancera, P.A., et al. (2011). In vivo identification of tumor- suppressive PTEN ceRNAs in an oncogenic BRAF-induced mouse model of melanoma. Cell *147*, 382–395.

Krützfeldt, J., Rajewsky, N., Braich, R., Rajeev, K.G., Tuschl, T., Manoharan, M., and Stoffel, M. (2005). Silencing of microRNAs in vivo with 'antagomirs'. Nature *438*, 685–689.

Landgraf, P., Rusu, M., Sheridan, R., Sewer, A., Iovino, N., Aravin, A., Pfeffer, S., Rice, A., Kamphorst, A.O., Landthaler, M., et al. (2007). A mammalian microRNA expression atlas based on small RNA library sequencing. Cell *129*, 1401–1414.

Lewis, B.P., Burge, C.B., and Bartel, D.P. (2005). Conserved seed pairing, often flanked by adenosines, indicates that thousands of human genes are microRNA targets. Cell *120*, 15–20.

Li, X., Cassidy, J.J., Reinke, C.A., Fischboeck, S., and Carthew, R.W. (2009). A microRNA imparts robustness against environmental fluctuation during development. Cell *137*, 273–282.

Lujambio, A., and Lowe, S.W. (2012). The microcosmos of cancer. Nature *482*, 347–355.

Memczak, S., Jens, M., Elefsinioti, A., Torti, F., Krueger, J., Rybak, A., Maier, L., Mackowiak, S.D., Gregersen, L.H., Munschauer, M., et al. (2013). Circular RNAs are a large class of animal RNAs with regulatory potency. Nature *495*, 333–338.

Mendell, J.T., and Olson, E.N. (2012). MicroRNAs in stress signaling and human disease. Cell *148*, 1172–1187.

Mukherji, S., Ebert, M.S., Zheng, G.X., Tsang, J.S., Sharp, P.A., and van Oudenaarden, A. (2011). MicroRNAs can generate thresholds in target gene expression. Nat. Genet. *43*, 854–859.

Mullokandov, G., Baccarini, A., Ruzo, A., Jayaprakash, A.D., Tung, N., Israelow, B., Evans, M.J., Sachidanandam, R., and Brown, B.D. (2012). High-throughput assessment of microRNA activity and function using microRNA sensor and decoy libraries. Nat. Methods *9*, 840–846.

Pillai, R.S., Bhattacharyya, S.N., Artus, C.G., Zoller, T., Cougot, N., Basyuk, E., Bertrand, E., and Filipowicz, W. (2005). Inhibition of translational initiation by Let-7 MicroRNA in human cells. Science *309*, 1573–1576.

Poliseno, L., Salmena, L., Zhang, J., Carver, B., Haveman, W.J., and Pandolfi, P.P. (2010). A coding-independent function of gene and pseudogene mRNAs regulates tumour biology. Nature *465*, 1033–1038.

Rhodes, D.R., and Chinnaiyan, A.M. (2005). Integrative analysis of the cancer transcriptome. Nat. Genet. Suppl. *37*, S31–S37.

Salmena, L., Poliseno, L., Tay, Y., Kats, L., and Pandolfi, P.P. (2011). A ceRNA hypothesis: the Rosetta Stone of a hidden RNA language? Cell *146*, 353–358.

Seitz, H. (2009). Redefining microRNA targets. Curr. Biol. *19*, 870–873.

Tay, Y., Kats, L., Salmena, L., Weiss, D., Tan, S.M., Ala, U., Karreth, F., Poliseno, L., Provero, P., Di Cunto, F., et al. (2011). Coding-independent regulation of the tumor suppressor PTEN by competing endogenous mRNAs. Cell *147*, 344–357.

Tsai, W.C., Hsu, P.W., Lai, T.C., Chau, G.Y., Lin, C.W., Chen, C.M., Lin, C.D., Liao, Y.L., Wang, J.L., Chau, Y.P., et al. (2009). MicroRNA-122, a tumor suppressor microRNA that regulates intrahepatic metastasis of hepatocellular carcinoma. Hepatology *49*, 1571–1582.

Wee, L.M., Flores-Jasso, C.F., Salomon, W.E., and Zamore, P.D. (2012). Argonaute divides its RNA guide into domains with distinct functions and RNA-binding properties. Cell *151*, 1055–1067.

Zhang, W., Sargis, R.M., Volden, P.A., Carmean, C.M., Sun, X.J., and Brady, M.J. (2012). PCB 126 and other dioxin-like PCBs specifically suppress hepatic PEPCK expression via the aryl hydrocarbon receptor. PLoS ONE *7*, e37103.